LUNDS UNIVERSITET

Design of a Compound Planetary Gearset

Johan Dandanell Litzén

May 2024

Division of Machine Elements
Department of Mechanical Engineering Sciences
Faculty of Engineering
Lund University

ISRN: LUTMDN/TMME—5013—SE

Abstract

The ever evolving automotive industry is pushing for further electrification of the vehicle fleet and the need for new electric drivetrains is therefore in high demand. The Formula Student competitions have also shifted their focus towards electric vehicles where innovative and efficient drivetrains are premiered in the design events. This master thesis work aimed to continue the development of Lund Formula Students future AWD system by developing the planetary gearbox that connects the electric motors to the wheels.

System requirements were derived from previously recorded data and performance targets set by Lund Formula Student. Target gearbox mass, size, gear ratio and life expectancy were determined. A suitable gearbox layout was found and different design parameters were investigated to find how they could be utilized in the design process. An iterative process was used where gear teeth number, macro geometry and tooth flank modifications were simulated to find the best design. Design and simulations of the gearbox were conducted in the driveline simulation software MASTA. Design of surrounding components such as planet carrier, bearings and seals was also done.

The resulting design satisfied all the initial requirements of the gearbox. The gearset had sufficient safety factors in terms of bending and contact stress as well as scuffing. Transmission error was reduced by altering tooth flank modifications in order to limit the vibrations within the gearbox. A suitable gearbox oil was selected based on viscosity and anti-scuffing properties. Mass was reduced in the components through structural analysis in ANSYS and component stiffness confirmed using MASTA simulations.

Acknowledgements

This master thesis work would not have been possible without the support and help from numerous people. First of all I want to thank my supervisor Rikard Hjelm at the Division of Machine Elements. His knowledge of gear systems and assistance in structuring the master thesis work has been truly valuable.

Secondly I want to thank the mechanical team at BorgWarner Landskrona for the opportunity to conduct my master thesis work with their support. I want to thank Henrik Wendt for making sure I had all necessary resources available and ensuring that I stayed on track throughout the project. A special thank you goes to Sebastian Katra and his uninterrupted support during every step of the way. His expertise in gear design, vehicle knowledge and continuous design input has been instrumental to the outcome of this master thesis.

Finally I want to thank Lund Formula Student. The project has been my second home for almost four years, and it has been a place where i got to develop my engineering skills, learnt the true value of teamwork and meet some amazing people. This master thesis work is based on a lot of knowledge, design and data from previous work at Lund Formula Student. I therefore want to thank current and previous members of the team for their dedication and hard work that made it possible for me to take on this project.

Contents

Chapter 1

Introduction

Formula Student is a student competition where the task is to design, build and race a formula style race car in one year. Competitions take place around the globe with over 600 participating universities from all over the world. The team at Lund University have been building racing cars since 2006 and fully electric cars since 2020. In order to further develop the electric car concept, the team set out to develop an AWD drivetrain with in wheel motors. With one motor per wheel the total grip potential of all four tires can be utilized to accelerate and rotate the car. Full control of each wheel also opens up the possibility for very effective torque vectoring systems further elevating the dynamic car performance. Apart from increasing the performance on track, a more complex drivetrain concept will enable the team to score higher in the design event at competition. All-wheel drive combined with an effective control strategy of the torque management showcase a higher degree of engineering capability of the team.

This master thesis was conducted with support from BorgWarner in terms of simulation tools and advise from their drivetrain engineers. The master thesis aimed to find a gearbox design that would allow the system to deliver suitable wheel speed and torque from the electric motors. The main focus was to investigate gear design parameters and how they could be used to design a compact and lightweight gearbox following the requirements. Design of surrounding components such as shafts, bearings and seals will be presented in short.

Similar design projects of AWD drivetrains have been conducted by other Formula Student teams. Mao [1] designed a single stage planetary gearbox adjusting gear macro parameters for Warwick Racing. Aune [2] developed a system with a compound planetary gearbox including tooth flank modifications to achieve a low weight, efficient transmission system for Revolve NTNU Formula Student. In this master thesis work, the design choices and design parameters investigated were based on performance targets set by Lund Formula Student.

Figure 1.1: LFS23 at Formula Student Netherlands

Chapter 2

Requirements

The new AWD system considered for Lund Formula Student is vastly different from the previous design and the team had no previous experience implementing in-wheel motors. The requirements of the system were therefore based on estimations and assumptions in combination with data. Every single component of the gearbox had specific requirements in terms of function, load capacity and life expectancy. Each component requirement was however derived from the system requirements presented in table 2.1. Each requirement was ranked based on importance.

1. Critical - Required for an operable system
2. Desired - Wanted requirement for best performance
3. Preferred - Improved performance, not necessary

Table 2.1: Gearbox requirements

Requirement	**Value**	**Importance**
Rules compliant	-	1
Life expectancy	1000 km	2
Gear ratio	1:12 - 1:13	2
Gearbox diameter	122 mm	1
Gearbox length	118 mm	2
Mass	22,4 kg	3
Load cases	Safety factors	1

2.1 Predetermined requirements

The AWD system is to be used in a Formula Student car and was therefore designed in accordance to the Formula Student rules. At the time of design the latest set of rules were the 2024 v1.1 [3], if the system is to be implemented at a later date rules compliance with the current rules must be checked.

The powertrain system will consist of a high voltage battery, inverters and four traction machines used as motors placed at each wheel. The battery will be capable of 600V, with total power from the battery limited to 80 kW according to the Formula Student rules. The traction machine that is to be used is the Fisher TI 085. It has a maximum torque output of 29 Nm and a 20 000 rpm limit, assuming field weakening is active. Without field weakening the motor speed limit is significantly reduced.

Size and geometrical limitations of the system were constrained by the wheels and brake calipers to be used. The design had to accommodate OZ Formula Student Magnesium CL 10” wheels and AP Racing CP4227-2S0 brake calipers. Size was also limited by the suspension components that had to fit inside the

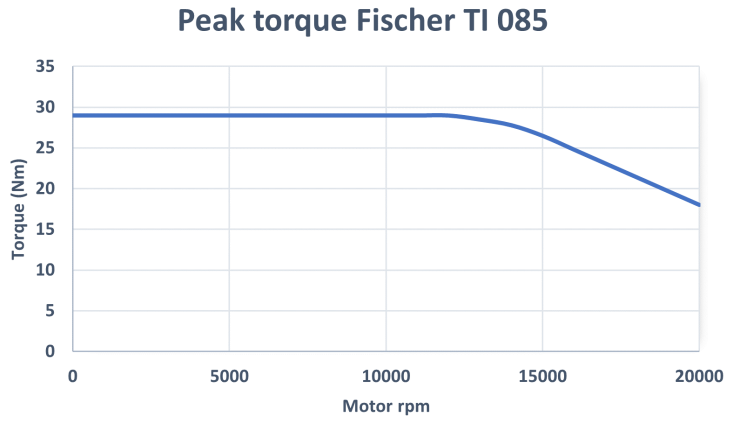

Figure 2.1: Peak torque curve Fisher TI 085 motor assuming field weakening

wheel and clear surrounding components during turning and wheel travel. The tires used were Hoosier 16" with a loaded tire radius of 194 mm.

Life expectancy of the system was two full seasons of testing and competition without having to replace any major components such as gears or planet carrier components. Regular maintenance such as exchanging the gear oil and replacing highly loaded bearings was accepted. As the initial cost of implementing the proposed design would be relatively high, it was deemed reasonable to ensure that it lasts at least two seasons. Based on previous seasons a realistic target driving distance was around 500 km per season. The system was therefore determined to have the life expectancy of 1 000 km of driving, equivalent to about 24 hours of continuous running at endurance pace.

2.2 Gear ratio

The gear ratio was selected to ensure maximum acceleration while having a suitable top speed. In a Formula Student competition the highest speeds are typically reached during the acceleration event or at long straights on the autocross track. Results from the acceleration event at Formula Student East 2023 showed that the top five teams crossed the finish line with a top speed of 110 - 125 kph. A motor speed of 20 000 rpm and wheel radius of 194 mm result in the relation between top speed and gear ratio presented in figure 2.2, suggesting a gear ratio between 1:11.7 - 1:13.3 for a top speed of 110 - 125 kph.

Table 2.2: Formula Student East 2023 Acceleration event results [4]

Team name	Car	Best time	Speed	Score	Place
Formula Student Team Delft	285	2,999	122,45	75,0	1
GreenTeam Uni Stuttgart	426	3,315	120,81	54,6	2
Revolve NTNU	463	3,360	114,65	52,0	3
FS Team Tallinn	424	3,409	118,42	49,2	4
TU Wein Racing	241	3,480	112,5	45,4	5

A vehicle model was built in the software OptimumLap to simulate different gear ratios and their impact on lap time. Parameters from the LFS23 car were used for mass, aerodynamic performance and tire data. Tire coefficient of friction was calculated from test data by dividing the lateral force with the normal force, it was assumed that lateral and longitudinal friction was equal (1,8 coefficient of friction). Drivetrain and motor parameters were chosen as an AWD system with an expected torque curve. The motor torque curve was calculated by using the Fisher TI 085 torque curve and multiplying the torque by four. For the RPM range

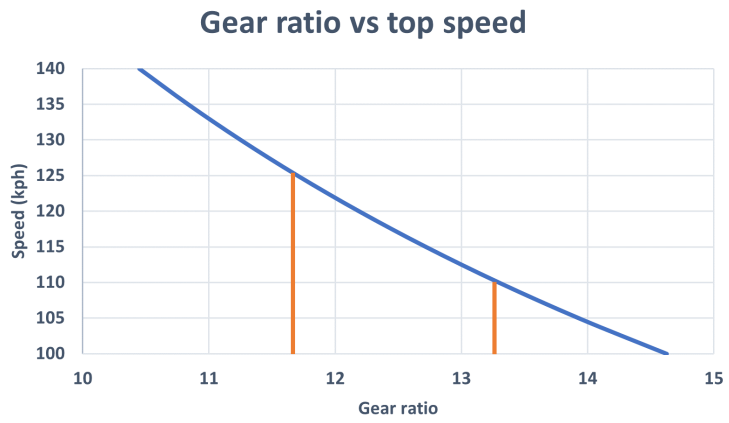

Figure 2.2: Gear ratio vs top speed

where the calculated power exceeded 80 kW, the torque was adjusted to 80 kW. This gave a rules compliant "allowed torque curve" that was used in the lap time simulations. Drivetrain efficiency was estimated to 97% and the power factor was set to 90% to account for losses in the inverter and motors.

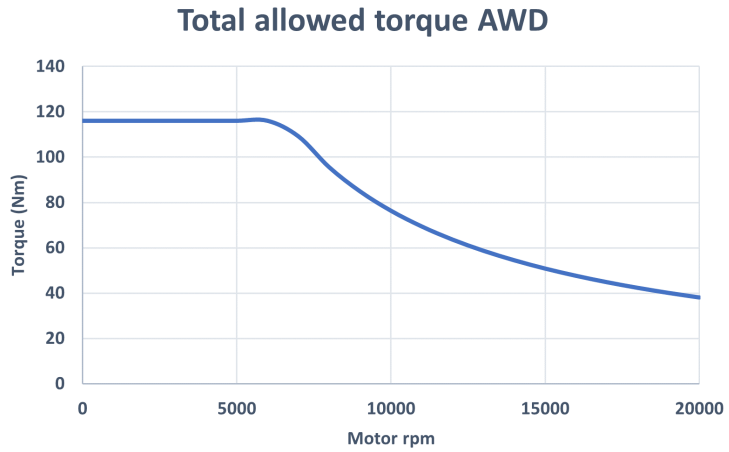

Figure 2.3: Allowed motor torque curve

In the simulations gear ratios were swept from 1:10 - 1:15. The results for acceleration simulations showed that a gear ratio between 1:12 and 1:13 had the lowest lap times. Simulations for autocross showed that a gear ratio below 1:13 had lower lap times. The target gear ratio was therefore set to within 1:12 - 1:13. The absolute lap time differences for different gear ratios appeared insignificant in the analysis. However, OptimumLap models the vehicle as a point mass without transient behaviour and assumes perfect conditions. Therefore the absolute values were not very interesting, rather the trend in performance increase was the relevant result.

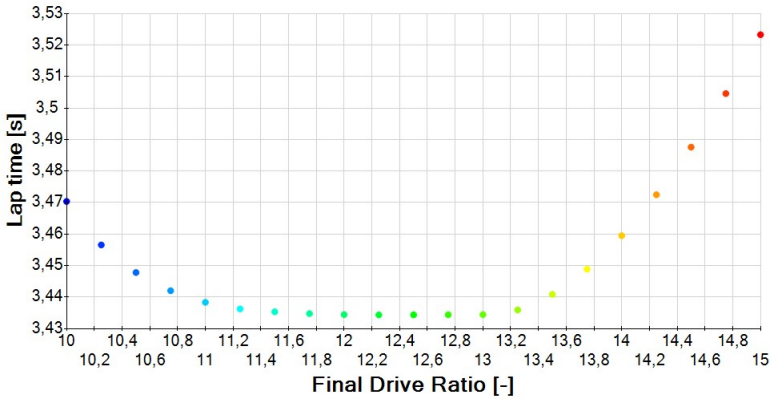

Figure 2.4: Acceleration gear ratio sweep

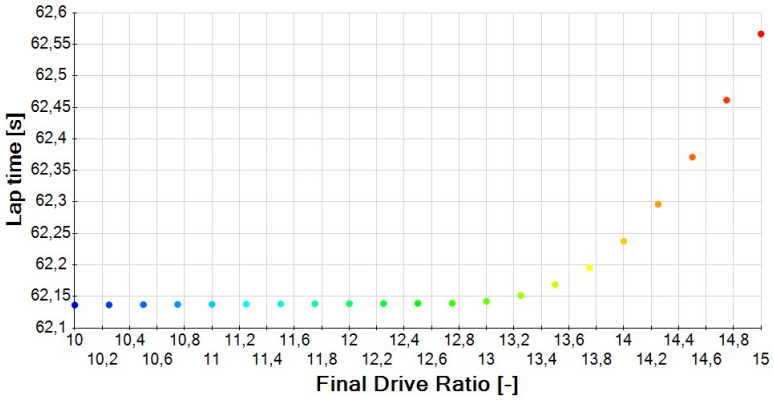

Figure 2.5: Autocross gear ratio sweep

2.3 Size

The available space for the gearbox was determined by the wheel, brake caliper and suspension components that had to fit inside the wheel. The brake caliper was placed as close to the wheel drum and spokes as possible, following the wheel manufacturers requirements. The resulting space in the wheel center determined the radial space available. Accounting for brake caliper mounting tabs on the upright and the hydraulic connectors that bolts to the brake caliper, the radial space available was 122 mm in diameter. Due to the necessary wall thickness of the upright and clearance between the gear teeth and the inside of the upright, the maximum swept diameter of the large planet gears was set to 115 mm diameter.

In terms of axial space, the gearbox had to be as short as possible in order for the motor to not interfere with the suspension rods during wheel movement. A kinematic analysis of the suspension was done by simulating 30 mm of bump and rebound travel combined with 30 degrees of steering angle in both directions. In order to have sufficient clearance between moving components a target axial size of the gearbox was set to 118 mm measured from the wheel center to the face of the electric motor.

(a) 122 mm diameter radial space

(b) 118 mm axial space

Figure 2.6: Available radial and axial space represented by the blue section

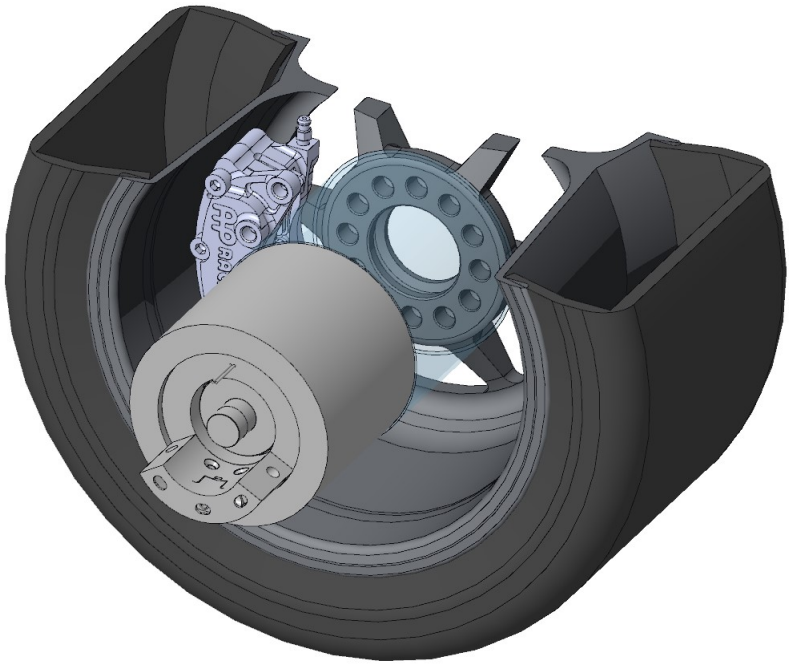

Figure 2.7: Available space for the planetary gearbox with electric motor

2.4 Mass

In terms of vehicle performance an overall low mass is favourable as it improves both lateral and longitudinal acceleration. As the gearbox is mounted to the upright assembly the mass is also unsprung, i.e. not supported by the suspension system. With increased unsprung mass the force from the suspension springs will accelerate the wheel and tire back into contact with the road surface slower, reducing tire grip. Due to the gearbox and motors being placed at each wheel the mass is also located far away from the rotational center of the car increasing the inertia. A higher vehicle inertia increases the yaw moment necessary for the car to rotate which will reduce cornering performance and make the car less agile. Placing a motor and gearbox at each wheel is inevitably going to reduce the suspension performance of a vehicle. In order to limit the negative effects on the vehicles dynamic properties, keeping the mass low was necessary.

Since there was no previous knowledge of this type of AWD system within Lund Formula Student, an accurate mass target was challenging to set. Despite the negative effects of increased unsprung mass, the AWD system would have the benefits of increased traction capabilities and the possibility to introduce torque vectoring. The increased tractive performance would likely increase overall car performance despite the higher unsprung mass. A reasonable target of not exceeding the LFS23 drivetrain mass was therefore set, the drivetrain of LFS23 including the motor had a mass of 22,4 kg.

2.5 Powertrain requirements

In order to find requirements for the new AWD system, data from the LFS23 car was used. The LFS23 car had a single EMRAX 228 electric motor connected to a Drexler limited slip differential through a chain and sprockets. Two drive shafts connected the differential with the rear wheels. Since the drivetrain concepts were vastly different, the data from LFS23 had to be modified and combined with estimations in order to be used for the AWD system. Parameters such as power, torque and wheel loads from LFS23 were found and converted to be applicable to the AWD system.

Data from a test session at Lockarps gokart track was used as the baseline. The test session took place mid-season where the car performed close to its peak performance without any issues. The data was therefore deemed suitable to use for development work. Data from the entire test session was analyzed and a lap that well represented the competition pace was selected to set the requirements.

2.5.1 Power

Calculations of power and torque produced by the motor were based on current measured by the BMS (battery management system), inverter voltage, motor rpm and an estimated efficiency of the LFS23 tractive system. Multiplying the motor torque with the gear ratio of the sprockets gave the torque at the wheels.

Adjusting the data from the single motor RWD system to the AWD system, the assumption that all power from the current system would continue to be applied at the rear wheels was made. Due to weight transfer during longitudinal acceleration the grip potential of the rear wheels will be higher compared to the front wheels, and more torque can be applied to the rear wheels without loosing traction. Therefore it was assumed that torque applied to the front wheels in most cases will be lower than torque applied to the rear wheels. Since the overall available torque will be higher with the AWD system, additional torque can always be applied to the front wheels compared to LFS23. But as previously mentioned it will be lower than at the rear wheels in most instances.

The torque was assumed to be split differently between the rear wheels depending on the driving scenario. During cornering the outside wheels have more potential grip due to lateral weight transfer and it was therefore assumed that as much torque as possible went to the outside wheel. The AWD motors have a peak torque of 29 Nm so in the case that the total torque output was higher than 29 Nm the rest would be applied to the inner wheel. During straight line driving it was assumed that the torque was split equally between the rear wheels. The definition of cornering was a lateral acceleration higher than 0,5 g.

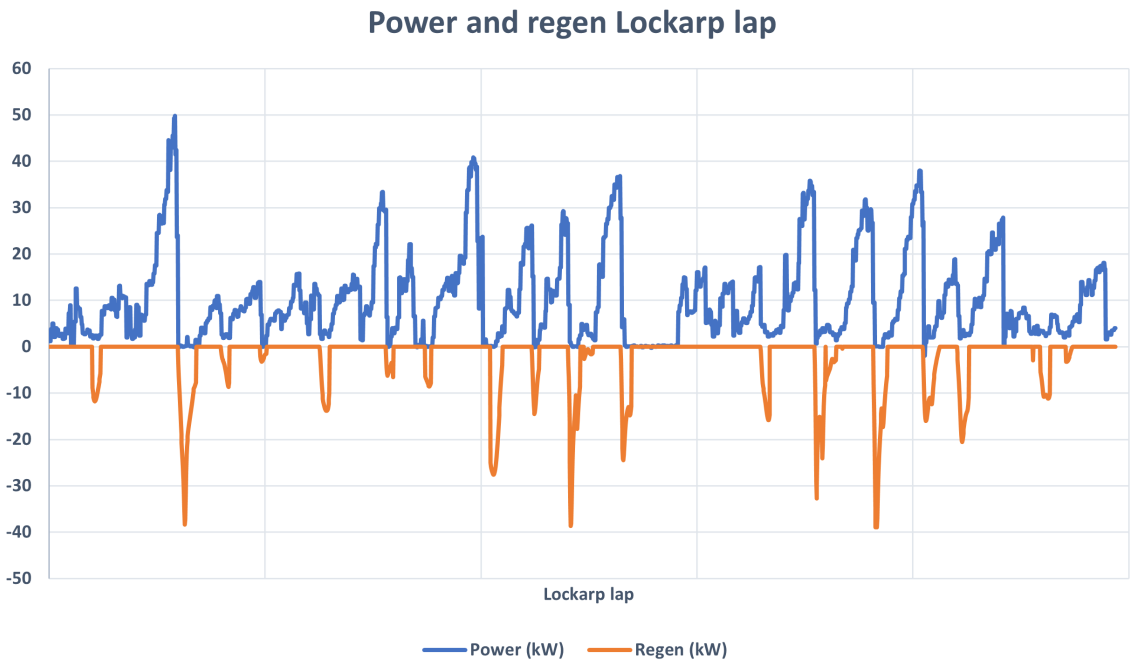

Figure 2.8: Driving power and estimated regenerative braking power of Lockarp lap

2.5.2 Regenerative braking

Regenerative braking is a way to recover energy during deceleration by using the traction machines as generators. Since LFS23 did not use any regenerative braking an estimation of how regenerative braking would affect the drivetrain system was done. The power necessary to either slow down or accelerate the car was calculated by finding the kinetic energy and the gradient of kinetic energy, which equals to the power slowing the car. Drag acting on the car will contribute to the deceleration and was therefore subtracted from the "slowing" power. Rolling resistance was deemed insignificant compared to braking power and therefore not accounted for. The resulting power was assumed to be available for regenerative braking.

During braking it was assumed that all resulting slowing power, up to the tractive system limit, could be recovered by the traction machines and would therefore apply a torque on the drivetrain. The tractive system limit was calculated to 39 kW ($65A * 600V = 39000W$, continuous charge current for the battery cells times total battery voltage) and all power above the limit was assumed to be absorbed by the mechanical brakes instead. With the regenerative power, torque at the traction machines and wheels could be calculated.

The torque from regenerative braking was split among the four wheels. Since a wheel with higher normal force generally has a higher friction force and therefore better braking capabilities, it was assumed that the regenerative braking torque was distributed equally to the normal force of the wheels.

2.6 Wheel loads

The planetary gearbox was integrated into the wheel assembly where the planet carrier served the purpose of wheel hub as well as carrying the planet gears. Due to this design, the planet carrier would be subjected to loads traveling from the contact patch of the tire, through the wheel and into the planet carrier before being transferred to the upright. As the forces on the wheel will cause bending loads on the planet carrier, potentially contributing to the misalignment of the gears, the wheel loads were included in the gear analysis.

Wheel load calculations were based on the testing data previously mentioned. Car parameters such as mass, mass distribution and suspension motion ratio combined with driving data enabled the car behavior to be determined. Driving data used were lateral, longitudinal and vertical accelerations, car speed and damper

sensor position. The normal force at each tire was calculated by multiplying damper position with spring rate and motion ratio. Force from the dampers was also included and determined through the damper movement speed and dyno plots of the speed/force relation of the specific Öhlins TTX 25 dampers.

With the tire normal forces determined, lateral and longitudinal tire forces could be calculated. To calculate the lateral and longitudinal tire forces an approximation of lateral and longitudinal force distribution was done by assuming that the distribution was equal to the normal force distribution. Multiplying the force distribution of each wheel with the car mass and lateral and longitudinal acceleration respectively, gave the forces at the tire. With tire forces known the moments induced on the wheel hub could be calculated and with that the reaction forces of each suspension component as well. Suspension loads and wheel loads were calculated for every data point of the lap.

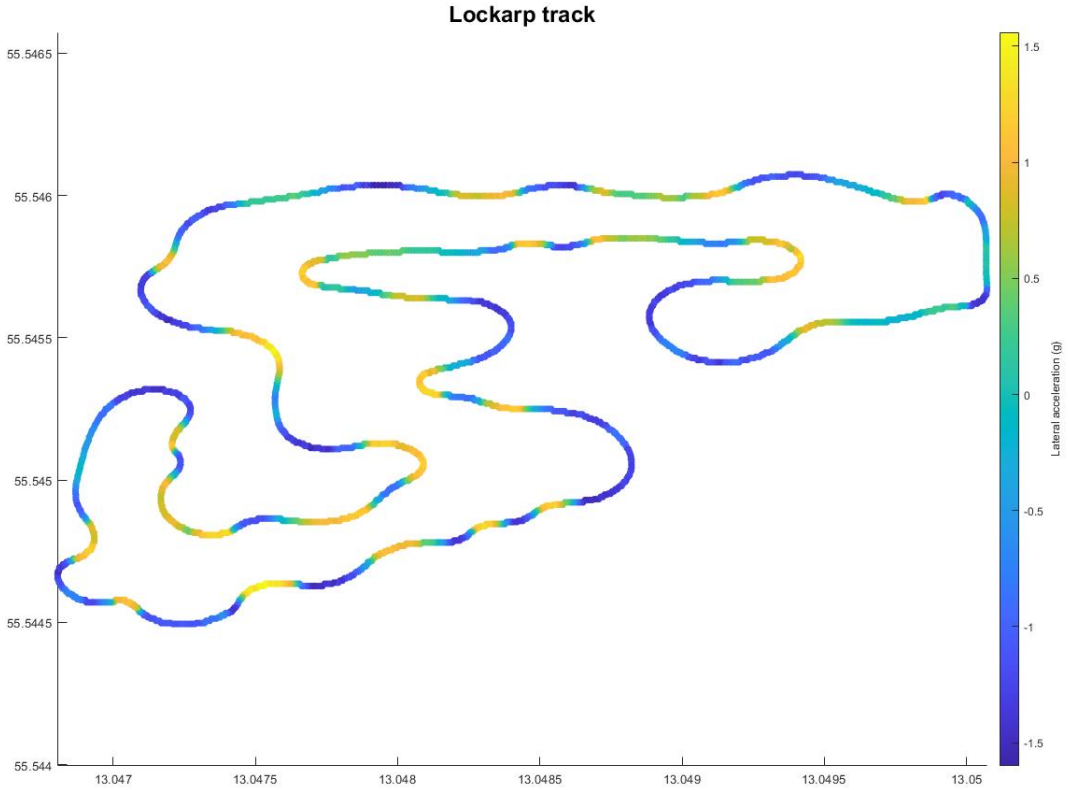

Figure 2.9: Lateral acceleration during the lap at Lockarps gokart track

2.7 Load cases

In order to accurately design the gearbox for its intended use, load cases representing different driving scenarios were constructed. The driving data from LFS23 was collected from an endurance test session, but could be used to estimate loads that occurs during autocross, endurance and skidpad driving. For other driving events and abuse cases, estimations were made based on previous experience.

2.7.1 Fatigue loads

Fatigue loads were the load cases expected to occur during autocross, endurance and skidpad running. The load cases contained a combination of motor torque and point loads applied to the hub interface.

Integration of the motor torque curves over the test lap showed that the rear left wheel experienced the largest amount of motor torque over a lap. Motor torque from the rear left wheel was therefore used for the fatigue load cases. When braking with regenerative braking the front wheels will experience a higher braking torque than the rear wheels due to the different grip levels, the regenerative braking capabilities are however limited by the tractive system limit. Comparison of peak torque from driving and estimated regenerative braking torque showed that the magnitude was similar. Using the rear left wheel torque would therefore not exclude any potentially higher torque peaks that could occur during regenerative braking at the front wheels. Considering the effects of regenerative braking, the rear wheels would still experience more frequent high torque and was therefore used to dimension the gears.

The number of load cases were selected to get a sufficiently accurate representation of the driving scenarios while not having too many cases resulting in unreasonable simulation times. 12 bins of motor torque load cases were created. 10 cases for drive in 10% intervals of maximum motor torque and two cases for regenerative braking in 50% intervals of maximum regenerative braking torque. Since drive torque occurred more frequently than braking torque and the time spent braking was less than time spent driving, more load cases for driving were created. In terms of contact stress on the gear teeth, only evaluating the drive torque would have been sufficient since the working flank changes during braking torque. But the bending loads cause stress in the root at both sides of the tooth, tensile and compressive stress respectively. Therefore, the occurrence of regenerative braking torque would contribute to the fatigue of the root and was therefore included in the load cases. In each bin created, the average motor torque and rpm was calculated.

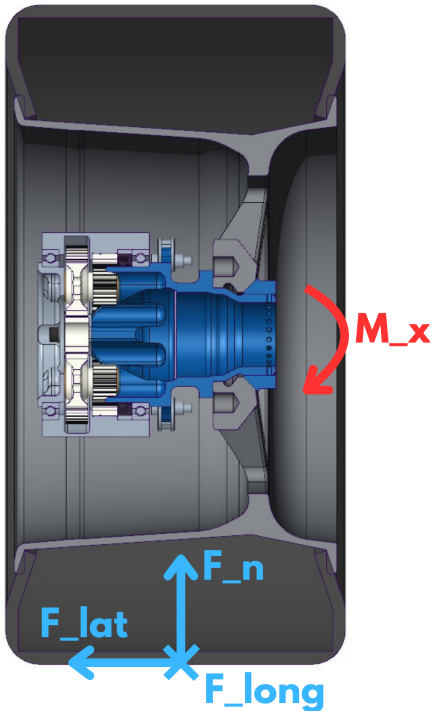

Figure 2.10: Forces acting on the tire, resulting moment M_x.

The point loads applied to the hub interface were the axial force, normal force and torque resulting from the lateral, longitudinal and normal force acting on the tire. Integration of axial force, normal force and torque on the hub over the test lap showed that the front left wheel experienced the largest amount of loads. Therefore, the front left wheel was used to dimension against tire loads.

For each bin of motor torque, five bins of point load cases were created. This was to capture the different point loads that occur in the torque intervals. The axial force, normal force and torque on the hub were placed into bins based on the torque M_x. M_x is the torque that causes the most bending loads on the hub due to the lateral and normal forces from the tire. The bins contained values from negative torque to 0%, 0 - 30% of max M_x, 30 - 60% of max M_x, 60 - 90% of max M_x and 90 - 100% of max M_x. The time spent in each load case was adjusted so that the total driving distance of all the load cases combined would equate to the target of 1 000 km.

The fatigue loads were based on data from two different wheels, front left for point loads and rear left for torque, see table 2.3. It can be seen as a worst case scenario where the highest load cases of motor torque

Table 2.3: Combination of data to dimension for fatigue loads

Motor torque	Rear left wheel
Point loads	Front left wheel

Table 2.4: 60 bins of load cases, 12 different motor torque cases combined with 5 point load cases

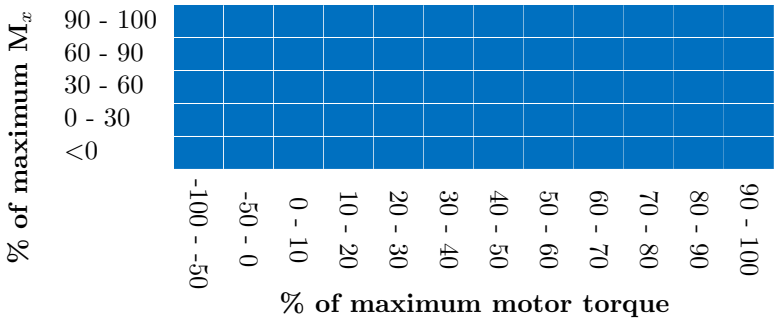

and point loads are combined. With this approach the gearbox would be dimensioned to handle both drive loads as well as loads from wheel forces. In reality a single wheel will most likely not see the loads combined in this way, but because of the many unknowns with this new type of drivetrain the approach was deemed reasonable. The 60 load cases of motor torque and point loads can be seen in table 2.4. Another scenario included in the fatigue load cases was driving over the infamous Formula Student Germany bump. Data from LFS17 showed a 2,2 g vertical acceleration traveling over the bump and it was assumed that the bump was hit 40 times for 0,5 seconds each time. In total 61 load cases for fatigue were created.

2.7.2 Acceleration loads

During the acceleration event, the powertrain is expected to deliver close to maximum torque to the motors in order to accelerate the vehicle as fast as possible. Operating gears at high speed and torque can lead to damage through scuffing, see section 3.3.3. Five load cases representing the peak motor torque curve from 12 000 to 20 000 rpm were created. The range from 0 to 12 000 rpm was excluded since less damage would occur in that range. It was assumed that 500 acceleration runs of four seconds each are run during the gearbox's life expectancy.

2.7.3 Abuse loads

The load cases representing fatigue loads and acceleration loads covers the expected scenarios that the gearbox could be exposed to. However, higher loads could occur during special circumstances. Driving off track, hitting curbs or large holes on track, or accidentally applying to much torque when bench-testing the system. In order to dimension the gearbox against these unexpected scenarios three abuse cases were constructed.

Two abuse cases for torque loads were created. The abuse cases were difficult to quantify since the cases represent unexpected events, however 1,6x maximum motor torque was deemed reasonable since it was well above the expected loads but without putting unnecessarily high demands on the gearbox. This load case roughly equated to running the system at 12 000 rpm, 100% torque from the motor and completely stopping wheel rotation with an external torque in 0,12 seconds. This estimation was done based on the drivetrain components inertia and rotational speed. A possible scenario where the load case could occur is spinning the car on track, reversing into a barrier that stops the wheel while still applying driving torque, unlikely but possible. The abuse drive case was 1,6x maximum motor torque in the drive direction and the abuse regen case (simulating regenerative braking) was 1,6x maximum motor torque in the reverse direction.

The third abuse load case was to capture extreme point loads and was constructed to represented a scenario combining the maximum lateral force of any tire from the test lap with a 2,2 g vertical acceleration caused by a bump. The normal force distribution at the moment of maximum lateral force was used to calculate the normal load. Driving torque from the motor at that moment was included as well. This load case was reasonable to assume since it assumed driving on the edge of the traction ellipse and simultaneously hitting a large bump. Braking forces were not included since it would overestimate the severity of the case in an unrealistic way. Including braking forces would reduce the lateral force since a part of the available traction would be necessary to facilitate braking. The lateral force on the wheel creates a larger torque on the hub compared to the longitudinal braking force due to the geometry of the wheel and hub. The lever arm of the lateral force is the tire radius while the lever arm of the longitudinal force is just the wheel offset. Therefore the braking scenario will not affect the system as much as the cornering forces.

Chapter 3

Gearset design

The design process of the gearset was divided into five stages; gear size selection, macro geometry design, tooth flank modifications, surrounding components and structural analysis. During each design stage, research, analysis and calculations were performed to find the important design parameters and how they could be used in order to fulfill the gearbox requirements. Several iterations of each design stage were performed with increased amount of components and complexity. The starting point was a simple gearset based on project course work "Design of a Compound Planetary Gearbox for a Formula Student Car", Litzén and Nilsson [5]. From the system requirements it was evident that a compact design capable of a high gear ratio was necessary to fulfill the specifications. Therefore, a compound planetary gearset with a large planet gear paired with the sun gear and a small planet gear paired with the ring gear was deemed to be the most suitable gearbox layout. The input shaft from the electric motor were to drive the sun gear and the planet carrier would act as the output shaft and be combined with the hub in order to drive the wheel. The ring gear would be held stationary, attached to the upright.

Once the requirements for a design stage were achieved the next stage was initiated, if no solution could be found the previous design stage was conducted again to find alternative solutions. The design flow chart on the next page give an overview of parameters adjusted during each design stage.

3.1 Design stage 1

Stage 1 of the gearset design aimed to find suitable sizes of sun, ring and planet gears with a layout that fulfilled the target gear ratio, dimensional constraints and had a possible mounting solution.

3.1.1 Gear size selection

The size of a gear is determined by the number of teeth and the normal module. Gearsets with different normal module and different normal module between the gear stages were considered early on in the design process. However, since each gear teeth design often require a unique cutting tool for manufacturing it was decided to keep the normal module equal between the gear stages and at a common size. The cost of tooling makes up for a substantial part of gear production when producing low volumes. Therefore the chances of finding a supplier that could manufacture the gears at a reasonable cost was deemed higher if the tooling cost could be kept low by selecting an appropriate normal module. The normal module was set to 1 mm for both gear stages for these reasons.

Suitable ranges of ring gear size, sun gear size and large planet gear size were selected, and for each combination a suitable small planet size was selected so that the center distance between the planet stages matched. The combinations resulted in approximately 25 000 gearsets. The gear ratio for all gearsets were calculated and filtered in order to find gear combinations with a gear ratio of the target ratio 1:12 - 1:13, 461 combinations were found.

The number of planets in a planetary gearbox can vary and is decided based on size constraints and structural requirements of the gearbox. In order to balance the forces of the meshing gears at least two

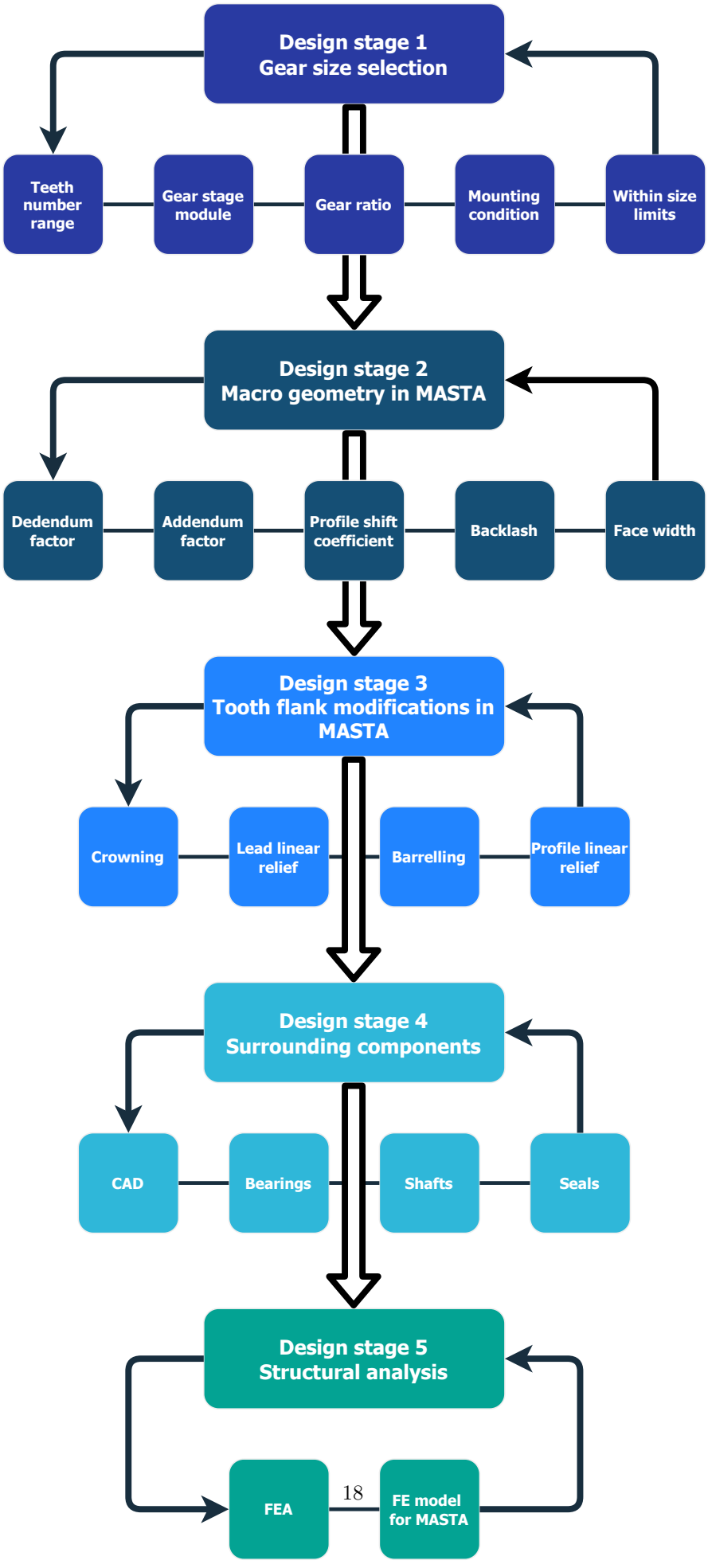
Design stage 1
Gear size selection
Teeth number range
Gear stage module
Gear ratio
Mounting condition
Within size limits
Design stage 2
Macro geometry in MASTA
Dedendum factor
Addendum factor
Profile shift coefficient
Backlash
Face width
Design stage 3
Tooth flank modifications in MASTA
Crowning
Lead linear relief
Barrelling
Profile linear relief
Design stage 4
Surrounding components
CAD
Bearings
Shafts
Seals
Design stage 5
Structural analysis
FEA
FE model for MASTA

planets are usually used. Adding additional planet gears reduces the amount of torque transferred between each meshing gear and could therefore be utilized to decrease gearbox size without loosing strength. With the selected gearbox layout, three planet pairs could be fitted while still maintaining room for the planet carrier to fit between the gears.

The gears of a planetary gearbox must be selected in such a way that they fulfill certain mounting conditions that allows the gearset to be assembled. For a single stage planetary gearbox, the planet gears can be assembled with equal spacing if the following condition is fulfilled [6]:

$$k = \frac{z_{sun} + z_{ring}}{n}$$

Where k is an integer, z is the number of teeth and n is the number of planet gears.

If the condition is not fulfilled the gears could still be possible to assemble, however not equally spaced. Instead each gear is assembled with an individual spacing k that fulfills:

$$k_1 + k_2 + \cdots + k_n = z_{sun} + z_{ring}$$

In a compound planetary gearbox it is possible to align the small and the large planet of each planet pair to each other in any way suitable to meet the mounting conditions. I.e. the teeth count does not affect the assembly as long as the center distances of both gear stages are equal. However, this could result in a design with three unique planet pairs that have slightly different rotation between the small and large planet. In the actual assembly of the gearbox, this could cause issues in terms of keeping track of which planet pair goes where and how they relate to each other. In order to ease assembly and to keep as many parts as possible interchangeable, individual planet pairs were to be avoided. Having identical planet pairs would also reduce the number of spare parts necessary, as each planet pair would not need to have its own spare.

To assemble a compound planetary gearset with identical planet pairs the following condition must be fulfilled:

$$k = z_{ring}\frac{1 - \frac{1}{R}}{n} + \frac{p}{R}\frac{z_{ring}}{z_{sun}}$$

Where k is an integer, p is an even number of teeth spaces and R is the fixed carrier ratio. The fixed carrier ratio for this type of compound planetary gearset is defined as:

$$R = -\frac{z_{ring}}{z_{SP}}\frac{z_{LP}}{z_{sun}}$$

Where SP denotes small planet and LP denotes large planet.

The 461 combinations of gears that offered a viable gear ratio were checked against the mounting conditions were 81 passed. Applying the size constraint of 115 mm swept diameter of the large planet gears reduced the results to 40 viable gearsets. Gear simulations of the initial stage 1 results showed that gear sizes below 17 teeth performed poorly in terms of bending and contact stress and sufficient safety factors could not be meet. Miler et al. [7] also suggests that gear sizes below 17 teeth should be avoided to avoid undercutting of the gear. The 40 viable gearsets were therefore filtered to remove results with gear sizes below 17 teeth. Four gearsets passed all the above mentioned criteria.

3.2 Design stage 2

During design stage 2 the gearsets found in stage 1 were evaluated in MASTA with the load cases described previously. The aim was to find a gearset with sufficient safety factors in terms of tooth bending and contact stress. Changes were done to the macro geometry in order to improve safety factors.

3.2.1 MASTA setup

MASTA is a driveline simulation software used to analyse and optimize gears, shafts, bearings and housings. Entire systems can be modelled and analyzed with specified load cases and detailed reports of safety factors, damage and life expectancy can be generated. The gear calculations are conducted according to ISO 6336. In MASTA a model of the entire gearbox could be constructed including the gears, shafts, bearings, and lubrication concept. Loads on the components were applied as input and output torques as well as point loads according to the constructed load cases. The analysis used in MASTA during design stage 2 was called "System Deflection" which is a finite element based static analysis. Deflection due to component stiffness and applied load is calculated for each component and connection in the system. Strength and damage calculations are then performed including the misalignment and deflections to account for the change in loading condition compared to the undeflected system.

MASTA evaluates safety factors of bending and contact stress for fatigue loading as well as static loading. The safety factors during static loading are calculated based on the material yield strength and the maximum nominal Von Mises stress caused by the load. The fatigue loading safety factors account for the material properties, geometry, method of construction and required lifetime. Fatigue strength is derived from the material S-N curve for the required number of load cycles. Due to the additional parameters accounted for, the fatigue safety factor display a more accurate calculation of the safety factor, therefore the fatigue safety factors were used to dimension the gears.

Safety factor limits were set in accordance to automotive business general guidelines for gear design: 1,2 for fatigue bending stress and 1 for fatigue contact stress. In design stage 2 however, slightly lower safety factors were accepted since no tooth flank modifications were added to the design. Adjusting the tooth flank modifications can improve safety factors significantly since the gear contact can be altered and issues like edge loading can be avoided. Since tooth flank modifications would be added at a later design stage and safety factors most likely be improved, lower limits were accepted.

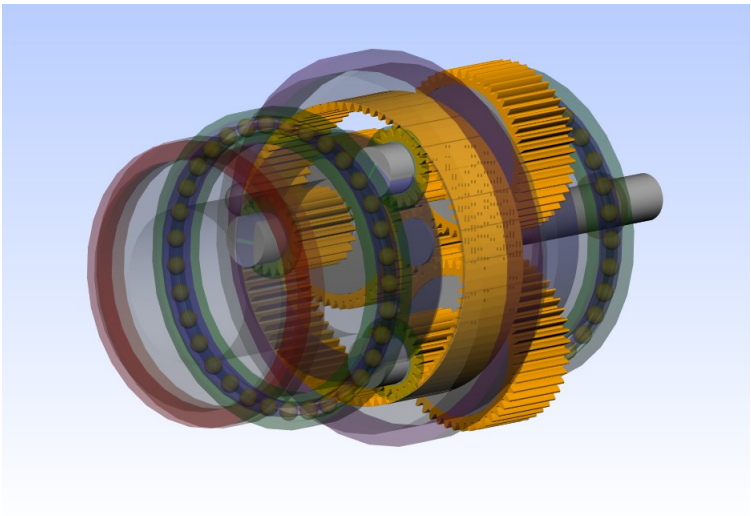

Figure 3.1: Baseline gearbox design in MASTA. Gears in orange, bearings in green and blue, output in red and housing in purple.

3.2.2 Macro geometry parameters

The macro geometry parameters that were adjusted during design stag 2 were gear material, gear quality, profile shift coefficient, addendum and dedendum distance, face width and backlash. Tooth chamfer was also added to protect the tip of the gears.

Gear material

For the sun gear and planet gears MASTA's default material was used, a case hardened (carburised) steel with material properties according to ISO 6336-5 [8]. During the case hardening process the material is heated to about 900°C and quenched. This process works well for the external gears because of the relatively large relation between cross section and diameter. For the internal ring gear however, the cross section is relatively small compared to the diameter resulting in a component more prone to warping during the case hardening process. Warping of the ring gear could ruin the geometrical accuracy and tolerances necessary for the safety factors. Therefore the material for the ring gear was specified as a nitrided steel. Nitrided steel does not have as good fatigue properties but since the nitriding process takes place at a lower temperature and without quenching, the geometrical tolerances can be kept higher.

Gear quality

Gear quality is classified according to different standards for tolerance requirements that have to be maintained during manufacturing. In MASTA the quality standard used was ISO 1328 [9] where the tolerance classes are numbered 1 to 11, in order of increasing tolerance. The standard dictates the allowed tolerances for geometrical properties such as pitch deviation, profile deviation, helix deviation and tooth thickness. Selection of the quality grade is a trade-off between geometrical accuracy and manufacturing cost, as a gear with very narrow tolerances will require more accurate tooling and machine time which increases cost. E.g. the fillet roughness was set at a higher value compared to the flank roughness. Due to this area not being used as a contact area, a rougher surface finish could be accepted which would ease manufacturing. The following quality properties were selected for all of the gears in MASTA.

Table 3.1: Gear quality grade according to ISO 1328

Helix quality grade	7
Pitch quality grade	7
Profile quality grade	7
Radial quality grade	7
Fillet roughness (R_z)	16 μm
Flank roughness (R_z)	3 μm

Profile shift coefficient

The profile shift coefficient x is a non-dimensional measurement of the displacement of the basic rack datum line radially from the reference cylinder of the gear. Having a positive profile shift moves the gear teeth radially outwards which results in an increased tooth thickness on the reference cylinder. Multiplying the profile shift coefficient with the normal module gives the profile shift in a unit of length. To keep the center distance between the gear stages constant, profile shift was adjusted to have the sum of profile shift between the gear pair to be zero. Adjusting the profile shift coefficients of a gear pair with this constraint results in an increased tooth thickness for one gear but a decreased tooth thickness on the reference cylinder for the other gear. The tooth strength increases with thickness and therefore amount of profile shift was a way to balance the safety factors between the meshing gears. Previous research by Miler et. al. [7] showed that including profile shift as an optimization variable can result in significant size and weight reduction in gear

pairs, a 33% reduction in volume by including profile shift was observed. With the limited design space and importance of a low mass, the advantage of including profile shift as a design parameter was evident.

Profile shift also alters the line of contact between the teeth affecting the amount of relative sliding. Sliding between gear teeth increases the contact temperature due to friction, high contact temperature can cause issues such as scuffing if the temperature increase is too severe. The amount of sliding can be determined with the sliding factor K_g according to ISO 21771 [10]:

$$K_g = \frac{v_g}{v_t}$$

Where v_g is the sliding speed and v_t is the velocity of the pitch circles.

Addendum and dedendum

The addendum and dedendum is the distance from the reference circle to the tip diameter and the distance from the reference circle to the root diameter respectively. As the addendum and dedendum parameters affect the height of the gear teeth the contact ratio is affected as well. Contact ratio affects both gear strength and efficiency and is therefore an important design parameter. Choi et. al. [11] found that including addendum and dedendum parameters could increase performance in terms of mass, efficiency and transmission error.

Backlash

Normal backlash is the distance between the gear flanks of the non-meshing side of the tooth. Backlash is required to ensure that teeth contact only occurs on the meshing flanks. The backlash has to be large enough to compensate for system deflection during load and ensure that no interference occurs, thereby preventing jamming of the gears. Since only one flank of each tooth is in contact if backlash is applied some delay will be introduced when driving direction changes. When the driving direction of the input changes each gear stage will have to rotate a certain angle to clear the backlash distance before the opposite flanks come into contact. This does not only reduce the response time of the system but also introduces shock loads in the teeth once the flanks come into contact. The aim was therefore to keep the backlash as low as possible without having interference. Changing the addendum and dedendum parameters had to be done in parallel with backlash changes in order to keep adequate clearance between the gears.

Face width

An increased face width of a gear pair results in a larger load carrying area and should theoretically for a given load result in lower stress. Results from the gear simulations revealed that an increase in face width only reduced stress up to a certain level. Contact charts were used to visualise the load distribution of the tooth contact surface. The results indicated that only part of the face width carried load when the face width was increased, see figure 3.2. The cause of the uneven loading was misalignment between the gears caused by deflection in the system. Components always deflect a certain amount under load and especially in a compound planetary gearset where the sun gear, ring gear and planets are not aligned axially. The load distribution can be altered with tooth flank modifications to get a more even load distribution. It was however found that compared to the initial design, face width could be decreased until no part of the tooth was unloaded at the cost of a slightly elevated stress level. With that, acceptable safety factors could be meet while minimizing axial width and subsequently weight.

In each gear pair one gear was designed with a slightly wider face width, the ring gear was wider than the small planet and the sun gear was wider than the large planet. Due to manufacturing and assembly errors the axial alignment in a gear pair could vary. With equal face widths of the meshing gears, one edge of each tooth will always overlap the flank of the other tooth and potentially cause edge loading if not axially aligned. Unequal face width ensures that potential edge loading only occurs in the narrower gear and can therefore be accounted for. With unequal face widths, an effective face width equal to the narrow gear can always be achieved. With equally wide gears the effective face width decreases if the gears are not aligned precisely, reducing the load carrying capabilities.

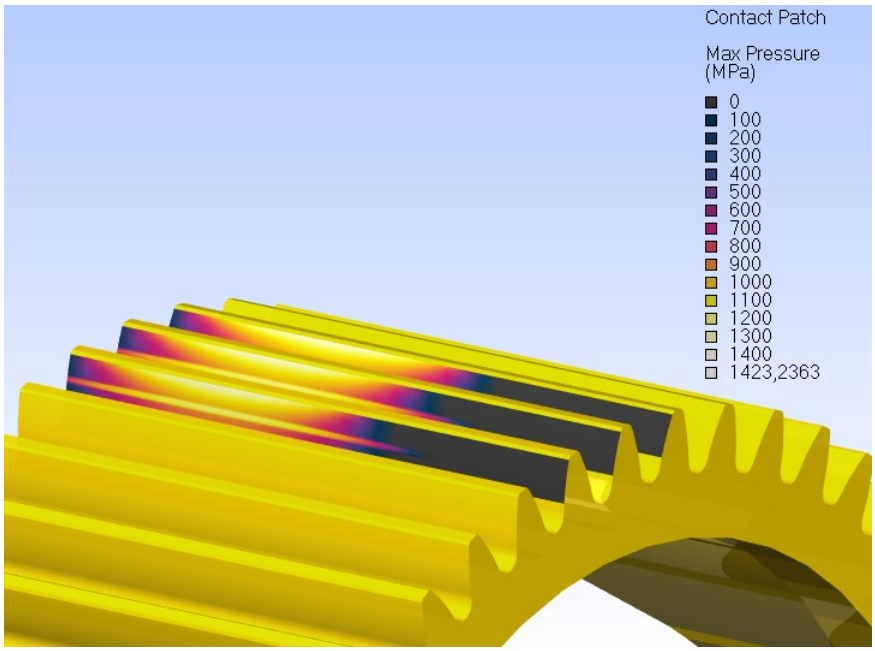

Figure 3.2: 3D view contact chart, partly loaded face width

3.3 Design stage 3

During design stage 3 tooth flank modifications were made to reduce edge loading, distribute the load more evenly on the teeth and ultimately increase safety factors. Apart from bending and contact stress, scuffing and transmission error (TE) was also investigated during design stage 3. In MASTA a micro geometry analysis was used to calculate the detailed load distribution between and along the gear teeth. The calculation splits each gear into independent strips with a constant combined mesh stiffness derived from the macro geometry. Tooth flank modifications, gear mesh misalignment and torque are included in the calculations where loads on each strip, contact patch and transmission error are derived.

3.3.1 Tooth flank modifications

Tooth flank modifications were done using four different parameters, crowning, barreling, lead linear relief and profile linear relief. The definitions are according to ISO 21771 [10].

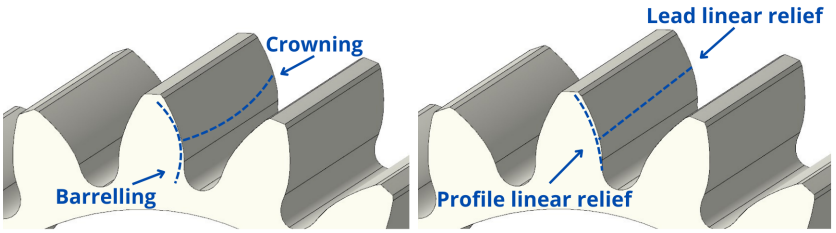

Figure 3.3: Tooth flank modifications

Crowning is an increasing relief of the tooth flank with a symmetrical parabolic shape. Crowning was used to reduce the risk of edge loading on both edges of the flank due to misalignment or manufacturing errors of the gear. Barrelling is a similar correction to crowning but applied to the tooth profile instead of the flank. Material thickness is reduced in a parabolic shape along the tooth profile. Barrelling moves the contact point towards the center of the profile away from the tip and root of the tooth.

Linear modifications to both the tooth flank and the profile was used to move the contact point with the highest stress point on the tooth surface. Lead linear relief extends across the whole face width of the tooth and decreases the tooth thickness linearly between the two profiles. Adding linear relief to the flank moves the contact point away from the starting point of the linear relief. Profile linear relief is instead applied to the tooth profile by reducing the tip thickness of the tooth. Altering profile relief moves the point of contact up or down the profile.

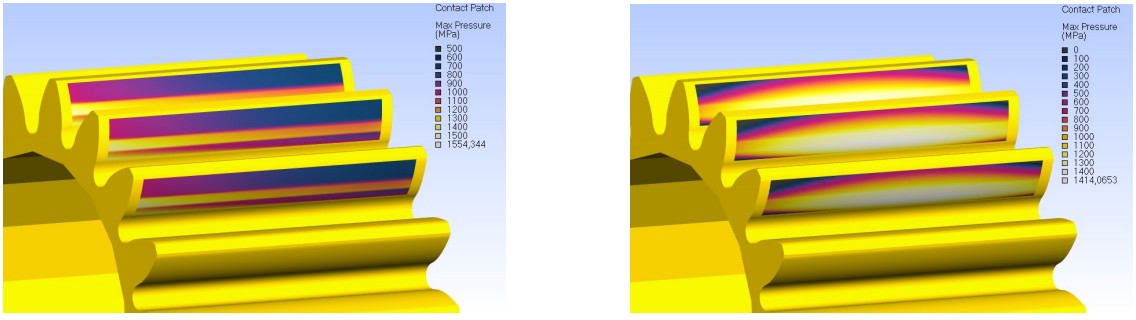

(a) No tooth flank modifications

(b) Final tooth flank modification

Figure 3.4: Contact between sun gear and large planet at maximum torque. More evenly distributed stress and lower peak stress after modifications, increased safety factors for bending and contact.

The four different parameters were used to alter the contact patch between the meshing gears. The target was to find a geometry with low maximum stress and evenly distributed stress across the entire flank

area. That way the full strength of each tooth could be utilized to carry load. The contact patch varied significantly with the input torque and since the load cases with high torque had greater accumulated damage, the geometry was modified to refine the contact patch at the high loads. From the initial results where no tooth flank modifications were added, both the input and output stages showed improved results. Safety factors were increased and the stress concentration moved towards the center. No tooth flank modifications were applied to the ring gear as the level of manufacturing difficulty significantly increases when adding modifications to the flank of an internal gear.

3.3.2 Transmission error (TE)

Transmission error is the deviation of the actual gear mesh position from the theoretical position that the gears would have occupied with a perfectly accurate geometry and infinite mesh stiffness. It is represented as linear motion along the line of action. Variation of the transmission error causes vibrations in the gearset that propagates and creates noise and gear whine. There are no noise regulations in Formula Student but gear whine could be distracting and tiring for the driver. More importantly however is to limit the vibrations as this can cause additional wear on the mechanical components of the gearbox [12].

When evaluating transmission error for a gear stage, the peak-to-peak value is of interest as the variation of transmission error is a major contributor to vibrations. A clear correlation could be seen between transmission error and number of teeth in contact which could be explained by to the change in mesh stiffness when the contact alternates between one or two teeth of engagement, see figure 3.5. When the transmission error increases the mesh shifts away from the ideal position and when the transmission error decreases the mesh shifts closer to the ideal position. This variation in offset from the ideal position will cause oscillations that due to the system inertia could create a superimposed torque. An oscillating superimposed torque could cause issues with driveability, torque management and additional component wear depending on the severity of the oscillations. The magnitude of this torque was unknown and it was realised that analysing it in full was beyond the scope of this master thesis work. However, limiting the peak-to-peak transmission error would have the benefit of reducing noise and reducing potential issues from the oscillations.

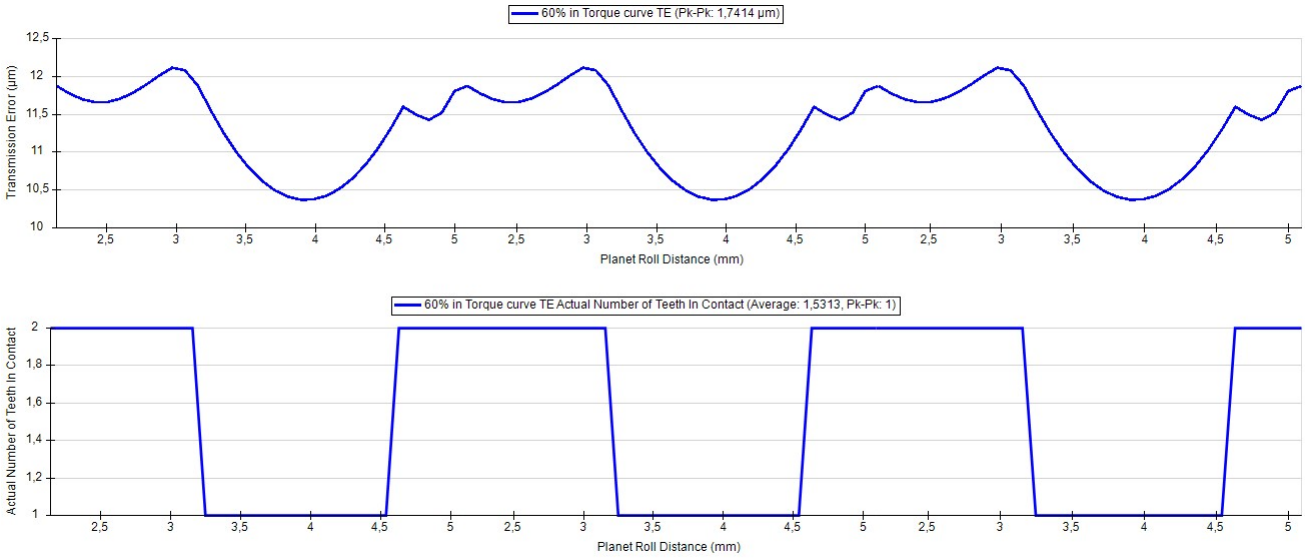

Figure 3.5: Correlation between TE and number of teeth in contact, output stage at 60% of max torque.

Transmission error is highly dependant on torque and gear tooth flank modifications. Transmission error was therefore analysed across the entire available torque range and tooth flank modifications were utilized to limit peak-to-peak TE. Reducing TE in one torque region would however often result in an increase of TE in another region. With the above reasoning that high peak-to-peak TE could cause additional wear, the

target was set to primarily limit TE in the torque range where the most gear teeth damage was accumulated, without negatively affecting bending and contact safety factors. The fatigue + acceleration load cases had the most damage in the high torque range 25 - 29 Nm, therefore peak-to-peak TE were to be limited in that torque range.

Table 3.2: Accumulated damage for load cases from the load cycles Fatigue loads + acceleration.

Load case	Contact total damage	Bending total damage
Fatigue 28,35 Nm 1	24,9 %	31,2 %
Fatigue 28,35 Nm 2	17,5 %	21,9 %
Acceleration 29 Nm	10,9 %	15,4 %
Acceleration 27,8 Nm	10,5 %	13,6 %
Acceleration 24,8 Nm	7,0 %	6,8 %

To reduce transmission error without lowering the contact and bending safety factors the effect of each tooth flank modification change had to be understood. A multitude of previous studies have indicated the positive effects tooth flank modifications could have on transmission error. Bonori et. al. [13] found that both linear and parabolic modifications of the involute profile could limit TE, Li [14] showed the effects of crowning on TE and Lei et. al. [15] showed examples of using linear tip relief and lead crowning in reducing TE.

In order to understand the effect of tooth flank modifications on the selected design different values of crowning, lead linear relief, barreling and profile linear relief were swept and the transmission error evaluated, figure 3.6 - 3.13. The sweeps for the input stage indicated that varied amount of crowning and lead linear relief had a relatively low impact on TE, changes in profile linear relief had very low impact on TE but changes in barreling had a significant impact on TE. The output stage sweeps showed very similar results. For the input stage 5 μm of barreling was deemed as an acceptable compromise between low TE in the high torque region and relatively low TE overall, an increase in barreling showed slightly lower TE at high torques but too much of an increase in TE over the rest of the torque range. Increased barreling showed no significant impact on the contact and bending safety factors. The TE impact of each tooth flank modification parameter was compared to the impact on safety factors and tooth flank modifications suitable for low TE with acceptable safety factors were selected for each gear stage.

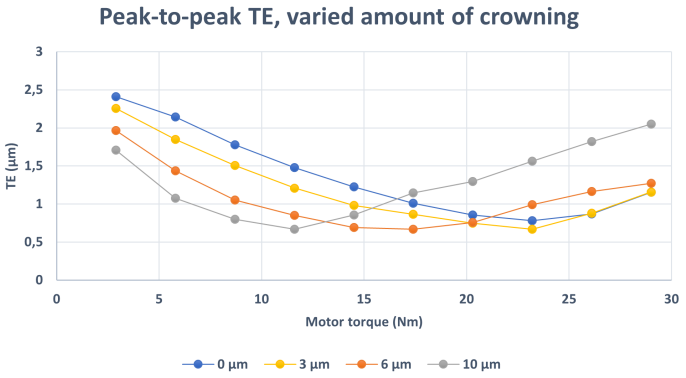

Figure 3.6: Input stage crowning sweep

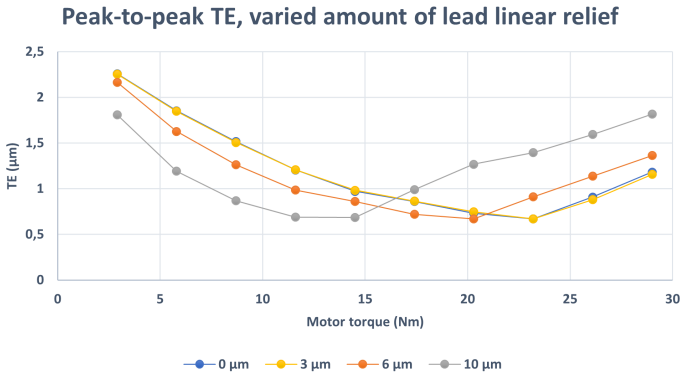

Figure 3.7: Input stage lead linear relief sweep

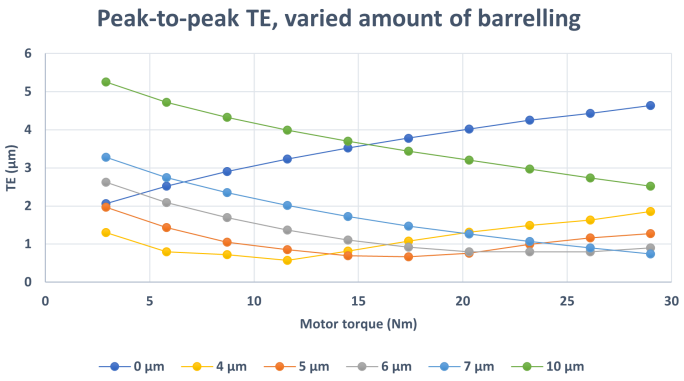

Figure 3.8: Input stage barrelling sweep

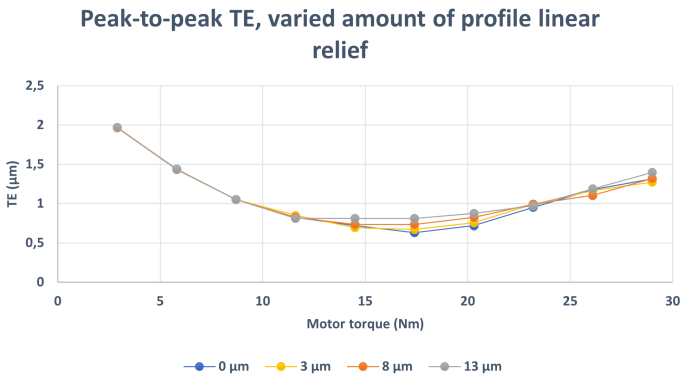

Figure 3.9: Input stage profile linear relief sweep

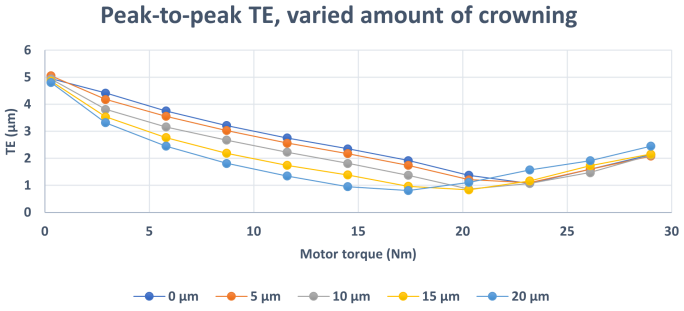

Figure 3.10: Output stage crowning sweep

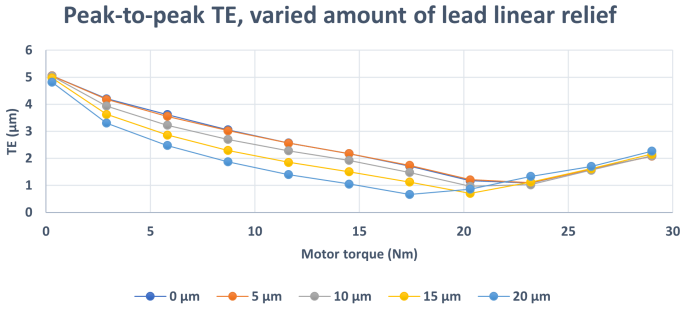

Figure 3.11: Output stage lead linear relief sweep

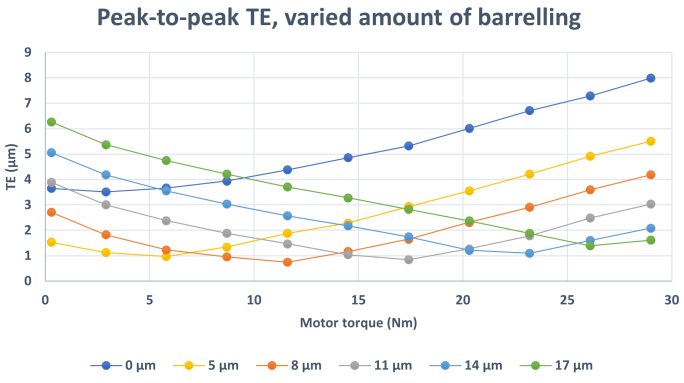

Figure 3.12: Output stage barrelling sweep

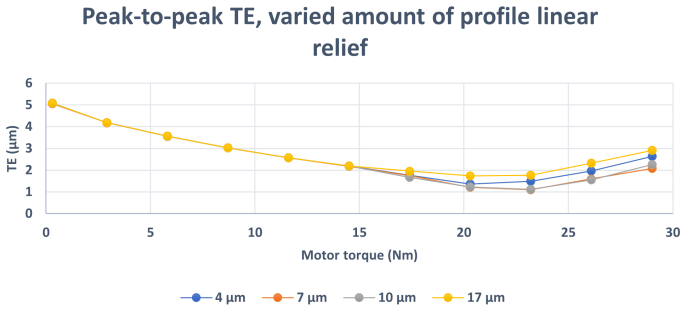

Figure 3.13: Output stage profile linear relief sweep

3.3.3 Scuffing

Scuffing occurs when the lubricant layer between the meshing teeth breaks down and the teeth flanks come into direct contact. The sudden increase of friction combined with the contact pressure and gear teeth sliding rapidly increases the temperature. The elevated temperature and contact between flanks can cause localized welding. When the flanks move out of the contact region the weld breaks, causing transfer of material between the teeth. The material transfer ruins the surface finish of the flanks and increase the risk of further damage. Unlike fatigue damage such as micropitting, damage from scuffing can occur momentarily by a single overload that breaks the lubricant film.

Profile shift can be utilized to limit the amount of scuffing. Reducing the gear sliding decreases contact temperature and thus reduces the risk of scuffing [16]. MASTA calculates the sliding factor at the tooth tip of each meshing gear. As the profile shift coefficient was altered, the sliding factor increased for one of the gears but decreased for the other. The change in sliding factor due to profile shift changes can be visualized by looking at the contact lines in figure 3.14. Increasing profile shift of the sun gear moved more of the contact lines inside the large planets reference circle. The further from the intersection between contact line and reference circle the more relative sliding between the gears occur. Keeping the contact lines more centered on the reference circle, which also keeps the sliding factors more equal between the gears, therefore reduces sliding.

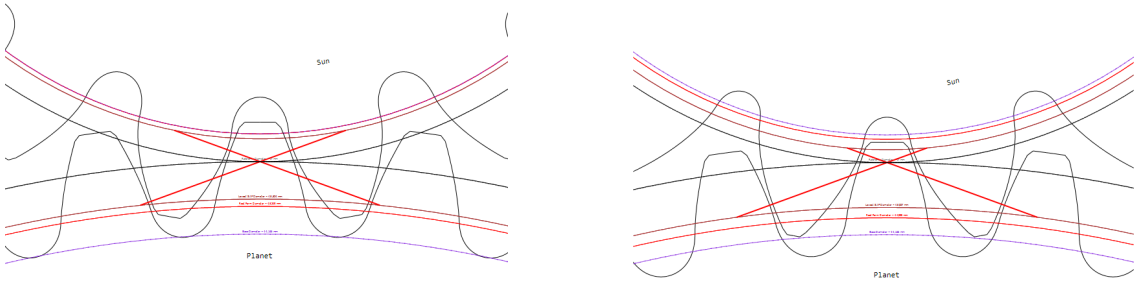

(a) Profile shift coefficient 0.13

(b) Profile shift coefficient 0.5

Figure 3.14: Contact lines between sun gear and large planet

Table 3.3: Sliding factor K_g at tooth tip for different profile shift coefficients x

	Sun gear	**Large planet**
$x = 0{,}13$	0,38	0,27
$x = 0{,}5$	0,48	0,13

Two methods of evaluating scuffing are described in ISO 6336 [17] [18], the flash temperature method and the integral temperature method. The flash temperature method compares the temperature at where scuffing is likely to occur, named the scuffing temperature, to the maximum contact temperature that arises during the gear meshing. Safety factor against scuffing according to the flash temperature method is defined as follows:

$$S_B = \frac{\Theta_S - \Theta_{oil}}{\Theta_{Bmax} - \Theta_{oil}}$$

Where Θ_S is the scuffing temperature, Θ_{Bmax} is the maximum contact temperature and Θ_{oil} is the oil temperature.

Θ_{Bmax} is calculated by adding the interfacial bulk temperature of the gears and the maximum flash temperature. The flash temperature is the increase in gear tooth surface temperature at a given point and based on several parameters such as coefficient of friction, material, rpm and load sharing factors.

The integral temperature method is based on the weighted average of the contact temperatures along the path of contact. Safety factor against scuffing according to the integral temperature method is defined as follows:

$$S_{intS} = \frac{\vartheta_{intS}}{\vartheta_{int}}$$

Where ϑ_{intS} is the allowable scuffing integral temperature and ϑ_{int} is the integral temperature.

The integral temperature method is less sensitive to cases with local temperature peaks that usually occur in gearsets with low contact ratios. Analyzing the planetary gearbox with both methods showed significantly higher safety factors with the integral temperature method, but since the gearset does have low contact ratios it is of interest to use the flash temperature method as well.

A lubricant's ability to inhibit scuffing can be tested using a FZG gear test rig. In the rig a gear pair is subjected to different loads at various speeds through predetermined load stages. After each load stage wear on the gear pair is measured and if the limit of wear is exceeded the test is terminated. The lubricant is then classified depending on the failure load stage. There are several different test protocols with different loads, speeds, lubricant temperatures etc. In MASTA the evaluation of scuffing is based on the FZG A/8.3/90 test where the maximum load stage is 14, the scuffing integral temperature and load stages for different test protocols can be seen in figure 3.15 from B.-R. Hoehn et. al. [19].

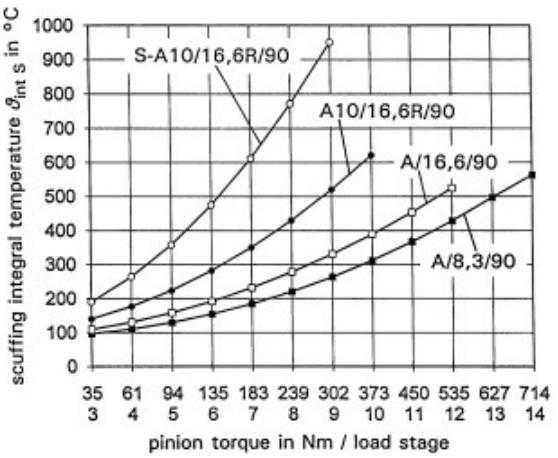

Figure 3.15: Comparison of scuffing test methods by B.-R. Hoehn et. al.

Many oils are classified using the American Petroleum Institute (API) GL ratings. FZG tests can be used to find the corresponding API GL rating of a lubricant. As seen in figure 3.16 below, a PASS at a specific FZG load stage corresponds to different API GL ratings [20].

According to Pan Ameriacn Lubricants FZG S-A10/16.6R/90 ls 9 PASS = API GL 5. FZG S-A10/16.6R/90 ls 9 has a scuffing integral temperature of 950°C which is significantly higher than FZG A/8.3/90 stage 14 (which is the method that is used in MASTA) that has a scuffing integral temperature of 580°C. According to ISO 6336-20 [17] and 6336-21 [18] a higher achieved FZG load stage result in higher scuffing temperature for both the flash temperature and integral temperature method, which in turn increases the safety factors against scuffing. Therefore the assumption that API GL-5 exceeds FZG A/8.3/90 stage 14 was made.

Scuffing load test	Flash temp. $\Delta\vartheta$ [K]
FZG (A/8.3/90) sls > 11	≈ 370
FZG (A/8.3/90) sls > 12	≈ 420
FZG (A/16.6/90) sls > 11	≈ 460
FZG (A/8.3/90) sls > 13	≈ 500
FZG (A/16.6/90) sls > 12	≈ 520
FZG (A/8.3/90) sls > 14	≈ 570
FZG (A/16.6/90) sls > 13	≈ 610
FZG (A10/16.6R/90) sls > 10 = API GL 4	≈ 620
FZG (S-A10/16.6R/90) ls 8 PASS = API GL 4	≈ 770
FZG (S-A10/16.6R/90) ls 9 PASS = API GL 5	≈ 950

sls = scuffing load step **ls = load step**

Figure 3.16: Classification of scuffing load test according to Pan American Lubricants [20]

3.3.4 Oil selection

Proper lubrication of the gearbox is essential in order to keep the bearings running smoothly and protect the contact surfaces of the gears. The oil forms a thin barrier between moving elements that reduce friction and creates a protective layer that inhibits metal to metal contact. Mitigating issues such as scuffing can be done by selecting the right type of gear oil. In the gear oil selection process three main parameters were considered; base oil, viscosity and additives. Availability and cost were also taken in consideration. Three different gear oils were found with different base oils and viscosity properties, see table 3.4.

Table 3.4: Evaluated gear oils

Oil	**Base oil**	**ISO viscosity grade**	**Standard**
Motul Gear 300 75W-90	Ester based	100	API GL-5
Klubersynth GH 6-22	Polyglycol based	22	<API GL-5
Castrol AP Gear 80W-90	Mineral oil	150	API GL-5

The base oil is either a mineral oil or a synthetic oil. Mineral oils typically have high pressure-viscosity coefficients allowing for greater film thickness at the operating viscosity. Synthetic oils can be tailored to very specific applications and often have better resistance to oxidation and thermal degradation. Synthetic oils can also have higher viscosity index which means that they are stable at a large temperature range. Keeping the viscosity low is desirable as it will generate less losses compared to a thicker oil, however it does compromise the load carrying ability as the oil is more prone to separating. Gear oils containing extreme pressure (EP) additives were selected as they provide additional protection of the surface. EP additives react chemically with the surface and create a sacrificial layer that inhibits metal to metal contact. EP additives, or anti-scuffing additives as they are sometimes refereed to, also help reduce the risk of scuffing due to the protective layer and the strengthening properties they add to the gear oil.

The three gear oils were evaluated by looking at the scuffing safety factors for all load cases. With the conclusion that the rating API GL-5 exceeds FZG A/8.3/90 stage 14 from section 3.3.3, the scuffing results are likely conservative. Since the calculations in MASTA are based on FZG A/8.3/90 the actual safety factors are likely higher.

The Motul oil performed best in terms of scuffing which partly can be explained by the base oil used. The ISO calculations off scuffing load capacity accounts for several lubricant parameters, one of them is the lubricant factor, X_L, which accounts for the base oil used, see figure 3.17. A higher lubricant factor has a positive impact on the safety factor.

The Klubersynth oil has a very low viscosity which is advantageous in terms of efficiency as the frictional losses will be lower. The safety factor against scuffing was however significantly lower than the Motul oil

Table 3.5: Scuffing safety factors and corresponding load case

Oil	**Scuffing safety factor**		**Worst load case**	
	Flash temp	Integral temp	Flash temp	Integral temp
Motul Gear 300 75W-90	1,32	3,94	16000 rpm, 24,8 Nm	14000 rpm, 27,8 Nm
Klubersynth GH 6-22	0,77	3,16	16000 rpm, 24,8 Nm	14000 rpm, 27,8 Nm
Castrol AP Gear 80W-90	1,01	3,63	16000 rpm, 24,8 Nm	14000 rpm, 27,8 Nm

$X_L = 1{,}0 \cdot (\eta_{oil})^{-0{,}05}$ for mineral oils;

$X_L = 0{,}6 \cdot (\eta_{oil})^{-0{,}05}$ for water soluble polyglcols;

$X_L = 0{,}7 \cdot (\eta_{oil})^{-0{,}05}$ for non-water soluble polyglycols;

$X_L = 0{,}8 \cdot (\eta_{oil})^{-0{,}05}$ for polyalfaolefins;

$X_L = 1{,}3 \cdot (\eta_{oil})^{-0{,}05}$ for phosphate esters;

$X_L = 1{,}5 \cdot (\eta_{oil})^{-0{,}05}$ for traction fluids;

Figure 3.17: Lubrication factors according to ISO 6336-20 [17]

and likely does not provide adequate protection of the gears. The results can likely be contributed to the polyglycol base oil, which lowers the lubricant factor, as well as the low viscosity which also lowers scuffing performance. The Klubersynth oil does not meet API GL-5 which further indicates that the protective performance is lower.

The Castrol oil performed worse in terms of scuffing compared to the Motul oil and had a higher viscosity and therefore higher efficiency losses.

With the results of the analysis, the Motul oil appeared as the best choice. However, physical testing should be performed to further evaluate the efficiency losses and performance at the proper operating conditions in terms of gearbox geometry and temperature.

3.4 Design stage 4

Design stage 4 included design of supporting parts around the gearset such as shafts, planet carrier, bearings and seals as well as additional features on the gears. Design considerations regarding the assembly process were also made during stage 4 to ensure accessibility for when the gearbox is to be assembled.

3.4.1 Gearset features

The planet pair will be manufactured in two parts welded together. The small planet gear and planet shaft featuring the needle roller bearing race will be machined before the gear blank of the large planet gear is pressed on to the shaft and welded around the outside seam. The large planet gear can then be machined. Attaching the large planet gear blank after the small planet gear is machined allows the gears to be mounted with minimum axial space between them without compromising the gear cutting process for the small planet.

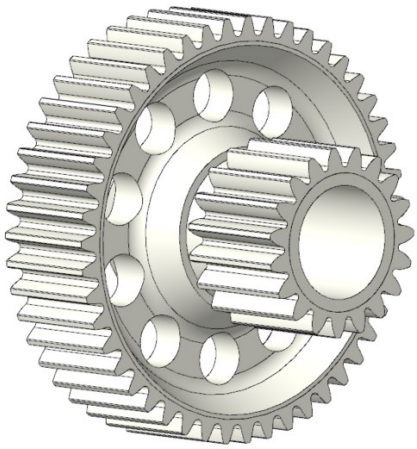

Figure 3.18: Planet pair and shaft design

The ring gear design features serrations around the perimeter locking the rotation of the ring gear. The ring gear will be pressed into the upright where the serrations will dig into the upright material and create a spline-like connection with interference fit on the serrations. The radial space occupied by the serrations is significantly less compared to having a flange where bolts or pins are used to secure the ring gear. The serrations do not go across the entire gear width as the un-serrated surface will be used to align the gear during the pressing operation. A slot behind the serrations was also added to make room for the excess material that is removed when the serrations in the upright are created.

The ring gear serrations were dimensioned with high safety factors as a failure in the serrated connection between upright and ring gear would be disastrous. The maximum torque acting on the serrations was assumed to be the abuse load case torque. The serrations were modelled as a rectangular beam with the parameters presented in table 3.6. The peak shear stress found was **130 MPa**. Since the sides of the serrations had a 20°angle the actual stress level should be even lower. Shear stress was calculated with the following formula:

$$\tau = \mu * \frac{F_s}{h * l}$$

where F_s is the force per serration.

$$F_s = \frac{T}{r_m * n}$$

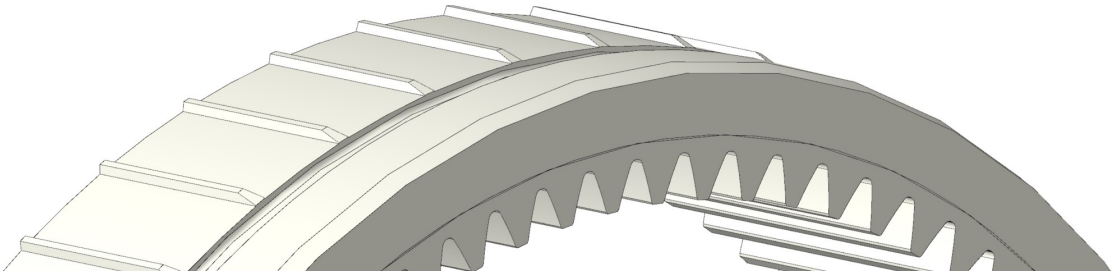

Figure 3.19: Ring gear serrations

Table 3.6: Serration parameters

Parameter	Symbol	Value
Number of serrations	n	50
Mean radius of serrations	r_m	48 mm
Height	h	0,38 mm
Length	l	7 mm
Cross sectional area	A	0,23 mm^2
Torque on ring gear	T	553 Nm
Rectangular beam shear coefficient	μ	1,5
Aluminium 7075 specific cutting force	$k_{c,1.1}$	800 MPa
Aluminium 7075 cutting force curve factor	m_c	0,25

The number of serrations and their geometry will affect the the necessary pressing force to mount the ring gear into the upright. To find the required force, cutting force for the material removed during the pressing operation was calculated. Cutting force was calculated using the following formula:

$$F_c = A * k_{c,1.1} * h^{-m_c}$$

Total cutting force was **11 260 N**. The actual pressing force necessary might be slightly higher due to friction between ring gear and upright. However, the magnitude of the force was deemed reasonable to achieve during the assembly process.

The radial slot for excess material had a volume of **223 mm^3**, the volume of material removed by the serrations was **80 mm^3**.

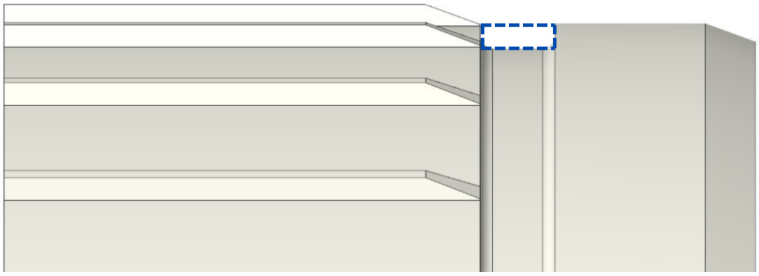

Figure 3.20: Ring gear slot for excess material

3.4.2 Bearings

Three different bearing types were used in the planetary gearbox. Two deep groove ball bearings to support the planet carrier in the upright, two needle roller bearings to support each planet shaft and axial thrust washers between planet shafts and planet carrier.

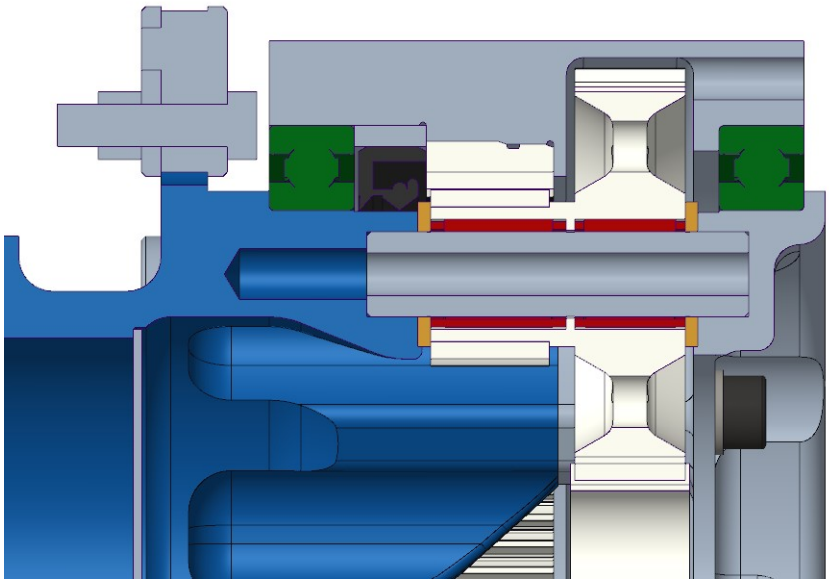

Figure 3.21: Planet carrier bearings in green, planet shaft needle roller bearings in red and axial thrust washers in orange.

Planet carrier bearings

The planet carrier bearings support the planet carrier and act as wheel bearings transferring loads from the planet carrier into the upright. A driving design consideration for the carrier bearings was the inside and outside bearing diameters. The outside diameter had to be large enough to allow assembly of the gearset in the upright, but within the gearbox size limitations. To limit axial size, the internal bearing diameter had to be large enough to fit outside of the planet pins, allowing overlap of components. The radial space was dictated by the gearset center distance, necessary stiffness of planet pins and material thickness of the carrier around the planet pins. The constraints required the bearings to have a maximum outside diameter of 118 mm and a minimum inside diameter of 80 mm. Both bearings had the same size constraints as components had to be assembled from both sides of the upright. Resulting bearing loads from the abuse wheel force load case were calculated with a free body diagram. Resulting radial forces were **3,9 kN** and **7,2 kN** for the outer and inner bearing respectively. Due to the relatively large size requirements all investigated bearing options could reach acceptable safety factors for the load cases. Bearings were evaluated based on size, weight, cost, load ratings and stiffness where the best option was found using an evaluation matrix, see table 3.7 and 3.8. NSK 6816 scored highest in the evaluation matrix and was therefore selected.

Table 3.7: Evaluated bearings. AC = angular contact bearing.

Model	Type	d (mm)	D (mm)	W (mm)	C (kN)	C_0 (kN)	Mass (g)	Cost (sek)
SKF 71816	AC	80	100	10	14,6	18,3	150	8 000
SKF 71817	AC	85	110	13	20,3	24	270	5 000
SKF 71916	AC	80	110	16	36,4	39	370	5 000
SKF 71818	AC	90	115	13	21,6	26,5	280	10 000
FAG 3816-B-2Z	Dual row AC	80	100	15	19,2	24,8	230	1 200
SKF 61816	Deep groove	80	100	10	12,7	11,2	150	1 200
NSK 6816	Deep groove	80	100	10	12,7	14,5	150	1 200

Table 3.8: Evaluation matrix of planet carrier bearings, not all bearings included. WR = weighted rating. *NSK 6816 received a cost rating of 6 since an existing team sponsor (Nomo) carries the bearings and they could therefore potentially be attained without cost.

		SKF 71816		FAG 3816-B-2Z-TVH		SKF 61816		NSK 6816	
Criterion	**Weight factor**	Rating	WR	Rating	WR	Rating	WR	Rating	WR
Size	0,3	5	1,5	4	1,2	5	1,5	5	1,5
Weight	0,25	5	1,25	3	0,75	5	1,25	5	1,25
Cost	0,2	1	0,2	5	1	5	1	6*	1,2
Load rating	0,15	3	0,45	4	0,6	1	0,15	1	0,15
Stiffness	0,1	4	0,4	4	0,4	2	0,2	2	0,2
Sum	1		3,8		3,95		4,1		**4,3**

Planet shaft bearings

Between the planet pin and planet shaft needle roller bearings without inner and outer rings were used. The bearings have high radial load carrying capacity and very small cross section. MASTA simulations with planet pins of different outside diameter indicated that 10 mm pins were necessary to have sufficient stiffness. Due to the small root diameter of the small planet gear the bearing cross section had to be as low as possible while maintaining an acceptable load rating.

For each planet shaft two needle roller bearings were selected. A SKF K 10X13X13 TN and a SKF K 10X13X16 TN, both with a 13 mm outside diameter and a 10 mm inside diameter but different widths.

Bearing calculations

Bearing calculations were performed in MASTA for the specified load cases to find safety factors for contact stress and life expectancy. Multiple calculation methods were performed, but "modified reference rating life" calculations in accordance to ISO/TS 16281 [21] were used to evaluate life expectancy. ISO/TS 16281 is an enhancement of ISO 281 [22] which includes the consideration of tilting and misalignment, operating clearance of the bearing and load distribution of the rolling elements. From the gearset analysis it was evident that misalignment occur between the meshing gears which particularly affects the needle roller bearings supporting the planet shaft. Therefore the ISO/TS 16281 method was deemed necessary to capture the impact of misalignment. Comparison of the results for the needle roller bearings between ISO/TS 16281 and ISO 281, showed significantly more bearing damage when misalignment was accounted for. Analysis of the abuse cases were done by evaluating the maximum contact stress instead of life expectancy. Maximum stress was more interesting since the abuse cases occur in a very short time period and significant bearing damage could occur by a single overload.

The simulation results showed sufficient safety factors for both NSK 6816 carrier bearings for the fatigue + acceleration load cases. Maximum contact stress could not be evaluated in MASTA for these particular

bearings, but calculations according to the manufacturers specifications indicated sufficient safety factors. At the average car speed and the abuse loads, the highest loaded bearing had a basic rating life of **155 hours**.

Table 3.9: NSK 6816 calculations based on abuse load case

Dynamic equivalent load	7154 N
Static equivalent load	7154 N
Basic rating life L_{10h}	155 h

Table 3.10: Bearing safety factors from MASTA calculations

Bearing	**Fatigue + acceleration** ISO/TS 16281		**Abuse loads** Max contact stress
	Safety factor	*Damage (%)*	*Safety factor*
NSK 6816 at wheel	13,22	0,04	-
NSK 6816 at motor	10,29	0,09	-
SKF K 10X13X13 TN	3,24	1,99	1,35
SKF K 10X13X16 TN	1,19	56,77	0,70

3.4.3 Seals

In order to retain the oil within the gearbox seals were used between the components surrounding the gearset. A rotary seal was required between the planet carrier and the upright preventing oil from exiting at the carrier bearing towards the wheel. At the motor side a rotary seal was used between the rotor shaft and motor bearing shield in order to prevent oil from entering the electric motor. An o-ring was used to seal the static motor housing against the upright. A lid bonded to the inside of the planet carrier was designed to prevent leakage through the hub.

When selecting the rotary seals gear oil compatibility and shaft speed were considered. Peripheral shaft speed at maximum motor rpm were 6,7 m/s for the planet carrier and 15,7 m/s for the rotor shaft from the motor. Conventional seals can typically handle speeds of 10 m/s which could be used for the planet carrier but not for the rotor shaft. For the planet carrier a Trelleborg TRA000800 FKM seal was selected and for the rotor shaft a Trelleborg TRAF00150 (Turbo seal) FKM capable of operating at higher speeds was selected. The material FKM is compatible with the gear oil used and can operate at temperatures of up to 200°C.

3.4.4 Planet carrier

The planet carrier was designed to serve the purpose of wheel hub and planet carrier. Featuring a wheel hub flange with drive pegs to mount the wheel against and a threaded stud for the center lock wheel nut. Mounting tabs for the brake disc were also included. The planet carrier had a two-piece design in order to allow for assembly of the gearbox. The components of the gearbox had to be assembled from both sides of the upright where the planet carrier would be bolted together around the components. Hollow pins were used around the bolted connection to ensure proper alignment between the halves. In order to comply with the Formula Student rules regarding positive locking on fasteners, safety wiring was used on the planet carrier bolts.

When selecting material for the planet carrier multiple factors had to be considered. Stiffness of the structure impacts the gear teeth loading. A compliant structure will allow for more misalignment between the gears which has to be accounted for when designing the gear geometry. Designing gears that can handle large misalignment will result in heavier and larger gears. In the perspective of gear design the stiffness of the carrier should be kept high. Simultaneously, the mass of the system should be kept as low as possible to

minimize inertia, efficiency losses and to keep the unsprung mass down. The relation between a material's stiffness and mass is called specific stiffness.

Table 3.11: Properties of viable materials

Material	**Density** (g/cm^3)	**Young's modulus** (GPa)	**Tensile yield strength** (MPa)	**Specific stiffness** ($10^6 m^2/s^2$)	**Specific strength** ($Pa * m^3/kg$)
Steel	7,9	200	670	25,3	85
Alu 7075-T6	2,81	72	503	25,6	203
Titanium GR5	4,5	112	880	24,9	196
Magnesium	1,74	45	200	25,9	158

Viable materials considered are presented in table 3.11. The materials were equally suitable in terms of specific stiffness. As the carrier would also act as the wheel hub, parts of the carrier would be loaded by the forces from the wheel. The region where the wheel and brake disc would be mounted does not require the same stiffness as around the gearset. Therefore this region was designed with material strength as the main consideration. In terms of specific strength aluminium 7075 and titanium GR5 have good properties. Aluminium is however more machinable and less expensive and was therefore selected.

A limiting design consideration was the manufacturing method of the carrier. Conventional machining was considered the most suitable in terms of cost and material. For the carrier half towards the wheel, the chosen manufacturing method set some limitations on how mass could be reduced. With the gearset center distance, required planet pin diameter and material thickness around the planet pins the radial space for a cutting tool to fit through was limited. From the wheel side of the component the radial space was limited by the hole through the threaded wheel nut stud. Available tool geometries from cutting tool suppliers were investigated and the design geometry was limited to allow machining with conventional tools.

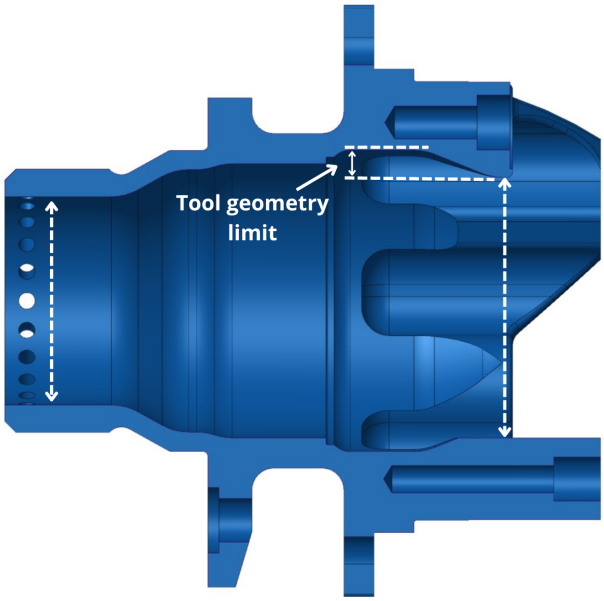

Figure 3.22: Manufacturing limitations on carrier geometry

3.5 Design stage 5

In design stage 5 the gearbox components were analysed in terms of structural integrity. Finite element analysis was used to reduce component mass while maintaining desired stiffness and strength. Finite element models of planet carrier, planet pins and planet shafts were produced and imported into MASTA. The finite element models contained information about the stiffness properties and was used in combination with the gear calculations to find the true deflection of the system. Thereby more accurately calculating the gear loads.

3.5.1 Mass reduction

In order to reduce mass of components multiple iterations of design stage 3, 4 and 5 were conducted. Once a suitable gear design was found in stage 3, geometry changes were done to either the carrier, planet shaft, planet pin etc. to reduce component mass. The mass reduced component was then converted to a finite element model and imported into MASTA to ensure adequate stiffness. Deflection values from the MASTA analysis could then be applied to the finite element model using structural analysis in ANSYS to find stress levels of the component. Once a geometry with acceptable stiffness and stress levels were found stage 3 was conducted again to adjust gear geometry.

Planet shaft mass reduction

Mass of the planet pair could be reduced by material removal at the midsection of the large planet gear. A high stiffness of the gears was desired in order to inhibit gear misalignment, by using an I-beam design for the large planet a high bending stiffness could be achieved while reducing weight. A 37% weight reduction of the planet pair compared to the solid gear blank could be achieved while maintaining adequate gear stiffness.

Planet carrier mass reduction

A high torsional stiffness between the carrier halves was necessary in order to limit the misalignment of the planet pins that were connected to both halves. As the materials contribution towards torsional stiffness increases with the diameter, material was removed in the center of the carrier while keeping more material towards the outside diameter. The planet carrier half towards the wheel also had to accommodate the wheel loads expected during driving. Apart from the stiffness evaluation in MASTA the carrier was therefore also analysed in ANSYS to confirm sufficient strength and stress levels. As the planet carrier would carry wheel loads and loads from the brake disc, further load cases were constructed which can be found in appendix A.1.

The planet carrier is constantly exposed to cyclic loading due to the rotation and varying wheel loads. The required life expectancy was relatively low but a simple analysis of fatigue life was conducted to ensure sufficient strength during the expected load cycles. No full fatigue load spectra was analysed, but selected loads from the fatigue load cases were investigated in order to find the corresponding stress levels. Material S-N curves illustrate the relation between the number of load cycles and the stress level until a material fails. Previous research suggests that keeping a stress amplitude below 150 MPa gives a life expectancy above 10^6 cycles [23][24][25], see appendix A.1. 1000 km of driving almost equals 10^6 revolutions of the wheel which means that force levels expected to occur every rotation of the wheel should not result in a stress higher than 150 MPa. With the use of material S-N curves life expectancy at specified loads could be found and geometry changes could be made to reduce mass while maintaining adequate strength.

Chapter 4

Results

From the gearset design stages a gearbox design fulfilling all specified requirements except one was found. During the abuse load case one of the needle roller bearings did not meet the safety factor for maximum contact stress and the ring gear contact safety factor was not met. They were however within an acceptable margin considering the assumptions and calculation methods used throughout the design.

Table 4.1: Gearset safety factors from MASTA

Abuse loads	**Sun gear**	**Large planet**	**Small planet**	**Ring gear**
Bending SF left flank	4,54	4,35	1,74	1,7
Bending SF right flank	4,54	4,35	1,74	1,7
Contact SF left flank	1,41	1,49	1,37	0,96
Contact SF right flank	1,41	1,49	1,37	0,96
Fatigue + acceleration loads				
Bending SF left flank	6,65	8,14	1,42	1,93
Bending SF right flank	2,91	3,55	4,17	5,35
Contact SF left flank	2,2	2,79	1,54	1,09
Contact SF right flank	1,25	1,58	2,76	1,94

In terms of gearbox size the final design had an outside diameter of 120 mm, 2 mm below the target and a length of 108 mm, 10 mm below the target. The gearbox mass was 1,57 kg and total mass with motor was 5,33 kg per wheel. Total drivetrain mass was 21,32 kg for all four wheels. The theoretical gearbox efficiency was 98,17% (see appendix A.3.1), overall gearbox efficiency from MASTA calculations was 98,34% but with a 99,08% efficiency at maximum torque, not accounting for lubrication losses.

Table 4.2: Gearbox design parameters

	Gearbox			
Gear ratio	1:12,54			
Center distance (mm)	32,5			
Efficiency (%)	98,34			
	Input stage		**Output stage**	
Normal module (mm)	1		1	
Normal pressure angle (°)	20		20	
Ratio	1:2,61		1:4,42	
Normal backlash (mm)	0,1		0,06	
	Sun gear	**Large planet**	**Small planet**	**Ring gear**
Teeth number	18	47	19	84
Face width (mm)	14	13	14	15
Profile shift coefficient	0,13	-0,13	0,45	-0,45
Tip diameter (mm)	20,46	48,54	21,7	83,03
Root diameter (mm)	15,48	44,14	17,4	87,5
	Tooth flank modifications			
Crowning (μm)	3	3	5	0
Lead linear relief (μm)	3	3	5	0
Barrelling (μm)	5	5	14	0
Profile linear relief (μm)	3	3	7	0

Transmission error was reduced in the high torque region as long as the bending and contact safety factors were not affected. Since the input stage of the gearbox rotate at a higher speed compared to the output stage the input stage transmission error will likely have a larger impact on the overall vibrations of the gearset.

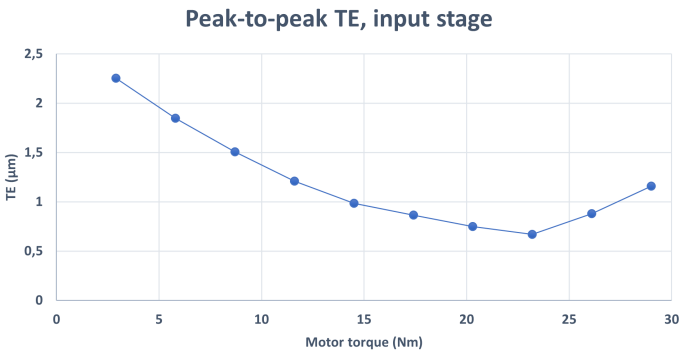

Figure 4.1: Input stage transmission error

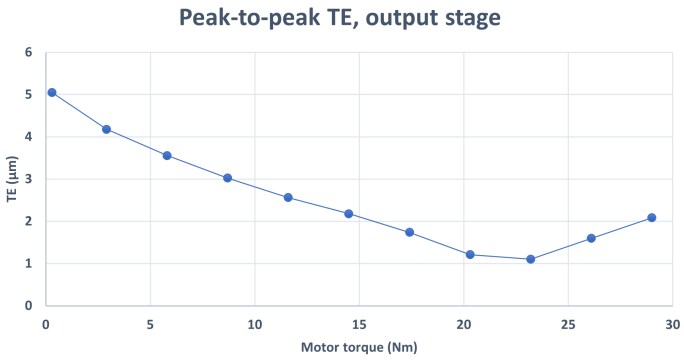

Figure 4.2: Output stage transmission error

Compared to LFS23 the new AWD drivetrain will not only replace the drivetrain components of 22,4 kg, but also the hubs and wheel bearings, with a mass of 2,97 kg, as they are integrated in the new design. The total mass of components that were replaced was 25,37 kg. The increase in unsprung mass of 18,35 kg was substantial but expected. The electric motors contributed with the majority of weight increase weighing 4 kg each, the added weight of the gearbox components were approximately 3,3 kg. Weight of all components can be found in the bill of material in appendix A.5.

Table 4.3: Change in system parameters between LFS23 and the new AWD system.
*Mass of comparable unsprung drivetrain components.

Parameter	**LFS23 RWD**	**New AWD system**	**Change**
System mass (kg)	25,37	21,32	- 4,05
Peak system torque (Nm)	674	1455	+ 781
Unsprung mass (kg)*	2,97	21,32	+ 18,35

4.1 Wheel loads

The initial hypothesis that wheel loads would contribute to gear misalignment and cause additional damage could not be confirmed in the simulation results. A comparison of the fatigue load cases with and without the wheel loads applied showed no significant difference in safety factors for contact or bending. The output stage right flank showed a 4,4% increase in contact safety factor for both the ring gear and one of the planet gears. This had no impact on the design as the right flank in the simulations is the active flank during regenerative braking, i.e. the flank that sees lower loads during the simulation. The safety factor with wheel loads were 2,76 and 1,94 for the small planet gear and ring gear respectively, way above the requirement. The low impact of wheel loads on the gear safety factors can likely be explained by the high stiffness of bearings and planet carrier, inhibiting excessive deflection of the planet shaft.

Table 4.4: Safety factor change (in %) with and without wheel loads for fatigue load cases

Fatigue loads (%)	**Sun gear**	**Large planet**	**Small planet**	**Ring gear**
Bending SF left flank	0,05	0,05	0,58	0,09
Bending SF right flank	0	0	1,28	0,21
Contact SF left flank	0,02	0,02	0,21	0,14
Contact SF right flank	0,01	0	4,4	4,4

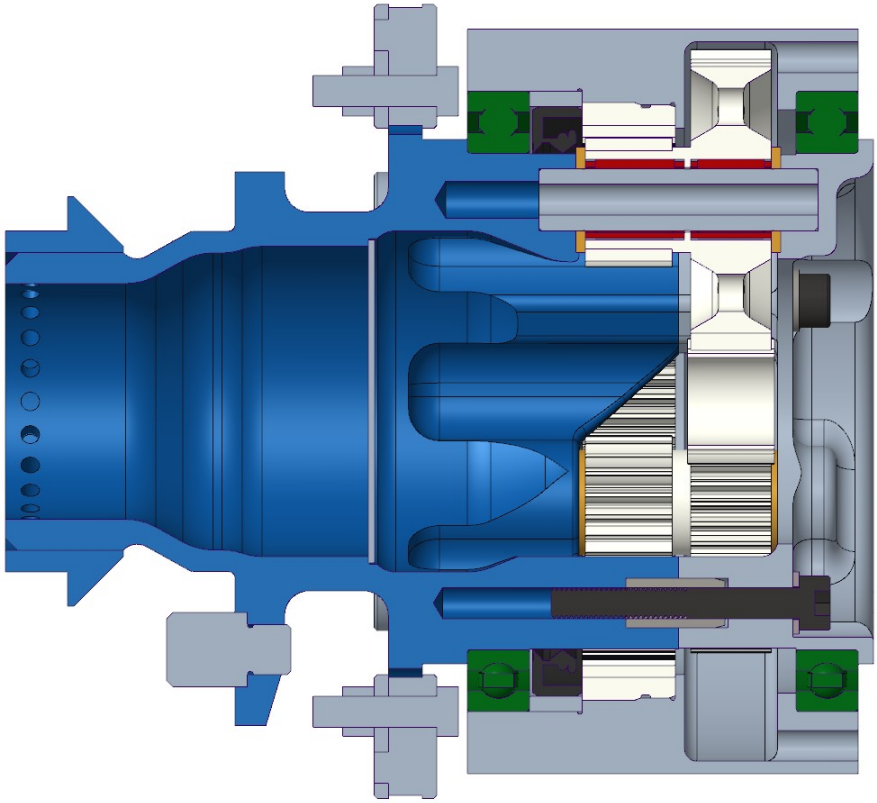

Figure 4.3: Planetary gearbox cross section view

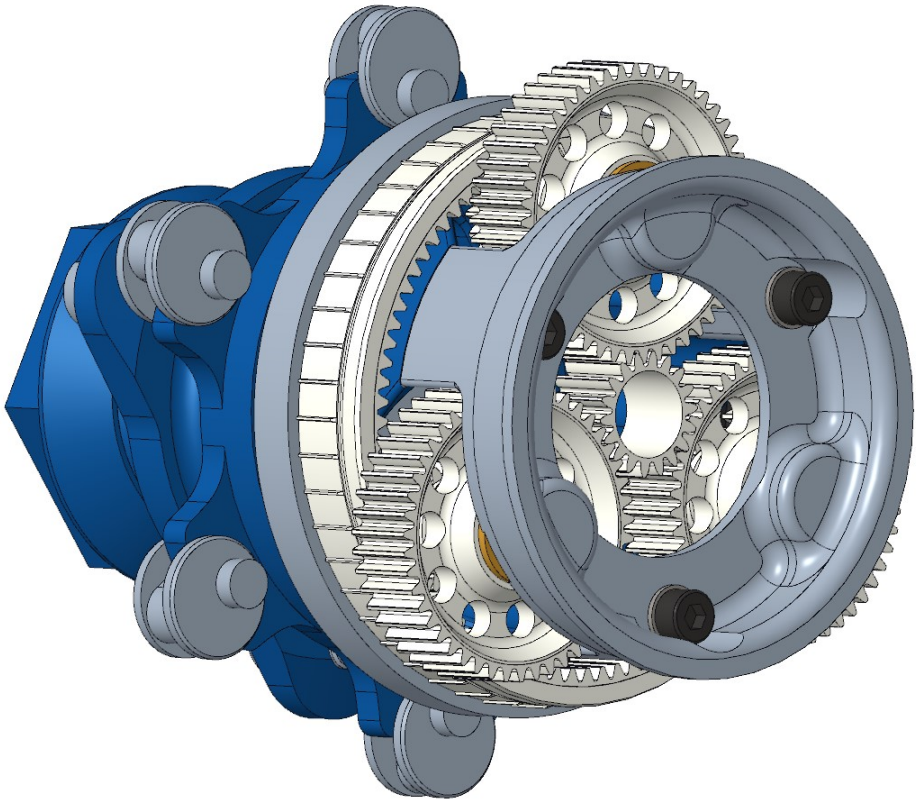

Figure 4.4: Planetary gearbox

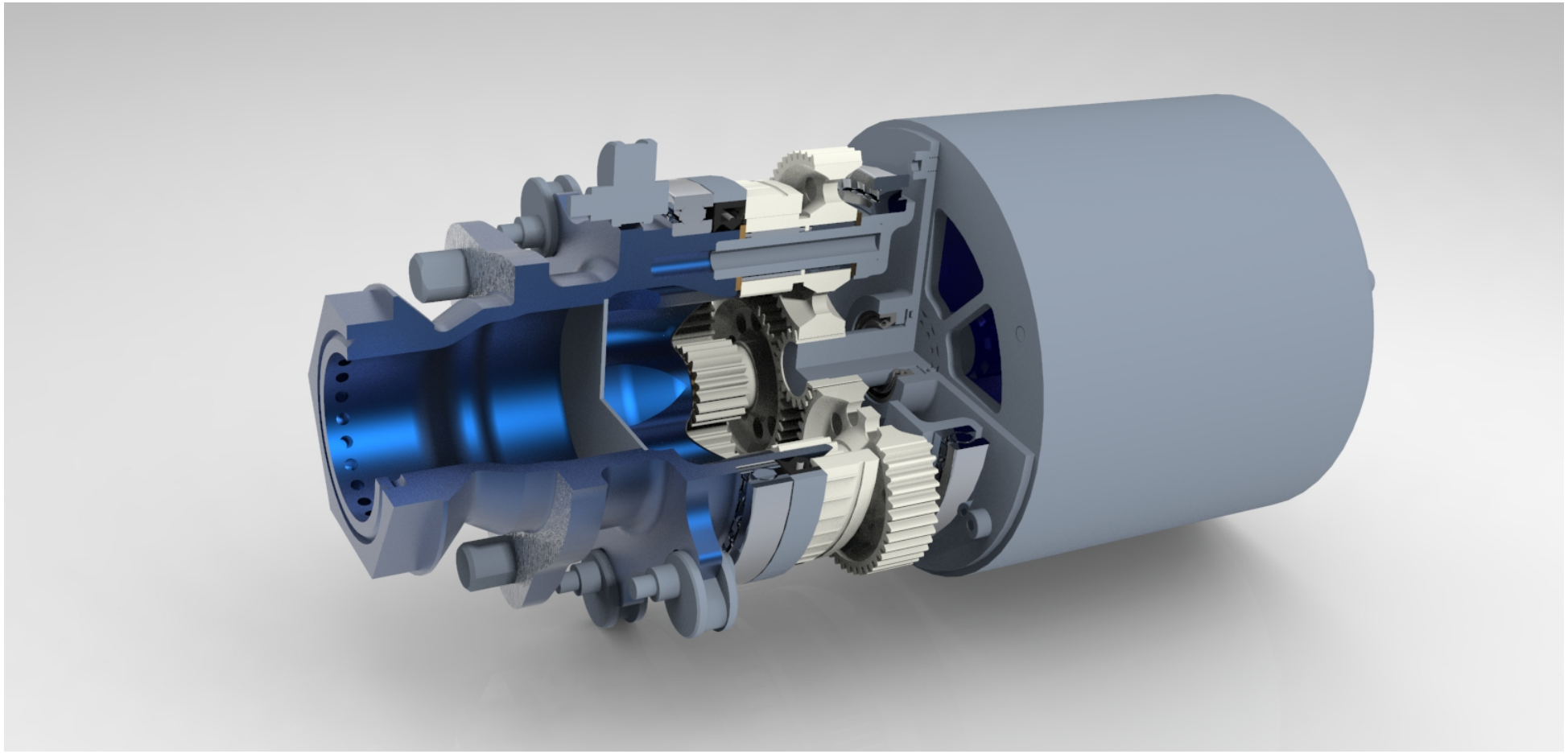

Figure 4.5: Planetary gearbox with traction machine

Chapter 5

Discussion

Final design results aligned well with results from Aune [2] in terms of size, mass and efficiency. A similar design approach was used and tooth flank modifications utilized to increase safety factors. Since some design requirements were different a direct comparison of detailed gear design was not relevant to do. The geometry modifications become very case specific and the assumptions are not similar enough to make that comparison. The system requirements are however quite similar, a gearbox with low mass, small size, gear ratio optimized for lap time with consideration to motor parameters and wheel size. The gearbox components are slightly different but a mass comparison between components serving equivalent purposes could be done. The mass from Aune was 1160 g and the mass from this work was 1113 g, a difference of 47 g. A table of the component mass comparison can be found in appendix A.4.

In terms of efficiency a slightly higher gearbox efficiency was found in this work, 98,3% compared to 97,8%. The efficiency was however just the gearbox efficiency, losses from lubrication, bearings and seals were not considered.

Compared to Mao [1] that designed a single stage planetary gearbox without any tooth flank modifications, results from this work indicated better stress distribution on the gear teeth. Altering the load distribution with the use of flank modifications reduced edge loading and ensured loading along the entire tooth profile. In Mao, less misalignment between the gears occurred simply due to the single stage layout, where some of the forces are balanced by the gears being aligned axially. But the difference between unmodified flank geometry and modified flank geometry could still be observed.

5.1 Gear safety factors

The gear strength calculations used in MASTA are based on ISO 6336. The calculations include a size factor that consider the influence of gear tooth size and the occurrence of weak points and defects. As material strength decreases with increased dimensions, the strength of a large gear tooth is comparably lower than a tooth with smaller module. According to ISO 6336-3 [26] a size factor below one is applied for gear modules above 3 mm and size factor equal to one for smaller gear modules. With the argument of decreased strength with increased tooth size the opposite should be true as well, increased relative strength with decreased module. Recent research have suggested complementary size factors to ISO 6336 for small modules to account for the increased relative strength. Concli [27] investigated the tooth root bending strength of gears with small modules for different steel grades, including both carburized and nitrided steels. Size factors above one were found for all investigated samples. Similarly, Hoehn et. al. [28] looked at tooth root bending, pitting, scuffing and wear of small module gears. Size factors above one for small module gears were found for both tooth root bending and pitting damage (contact).

For a normal module of 1 mm, as used in the gearset design, the research suggest a size factor for bending stress (Y_X) of 1,31 and a size factor for contact stress (Z_X) of 1,14. As the size factor is proportionately related to the safety factor, adjusted safety factors for normal module 1 mm could be calculated. With the adjusted safety factors all gears passed the required safety factors.

Table 5.1: Gearset safety factors adjusted for normal module 1 mm

Abuse loads	**Sun gear**	**Large planet**	**Small planet**	**Ring gear**
Bending SF left flank	5,95	5,7	2,28	2,22
Bending SF right flank	5,95	5,69	2,28	2,22
Contact SF left flank	1,61	1,69	1,56	1,1
Contact SF right flank	1,61	1,69	1,56	1,1
Fatigue + acceleration loads				
Bending SF left flank	8,71	10,67	1,87	2,53
Bending SF right flank	3,82	4,64	5,47	7,01
Contact SF left flank	2,5	3,18	1,76	1,25
Contact SF right flank	1,42	1,8	3,14	2,22

5.2 Bearings

The bearings with the worst safety factors from the MASTA simulations were the small planet needle roller bearing. Running the Fatigue + Acceleration load cases the ISO/TS 16281 modified reference rating life damage was 57%. The most extreme load was observed during the abuse drive case where the safety factor for maximum contact stress was 0,70 and the maximum normal contact stress was 4772 MPa. According to automotive business CAE guidelines the maximum element normal stress during 0,1% of the load spectra should be less than 4600 MPa. Since the abuse cases are expected to occur very seldom during the lifetime of the gearbox and a larger bearing could not be used without compromises to the size of the gearset, the decision was to continue with the specified bearing despite the low safety factor. However, if a abuse load case is suspected to have occurred during driving or testing, the bearings should be inspected or replaced.

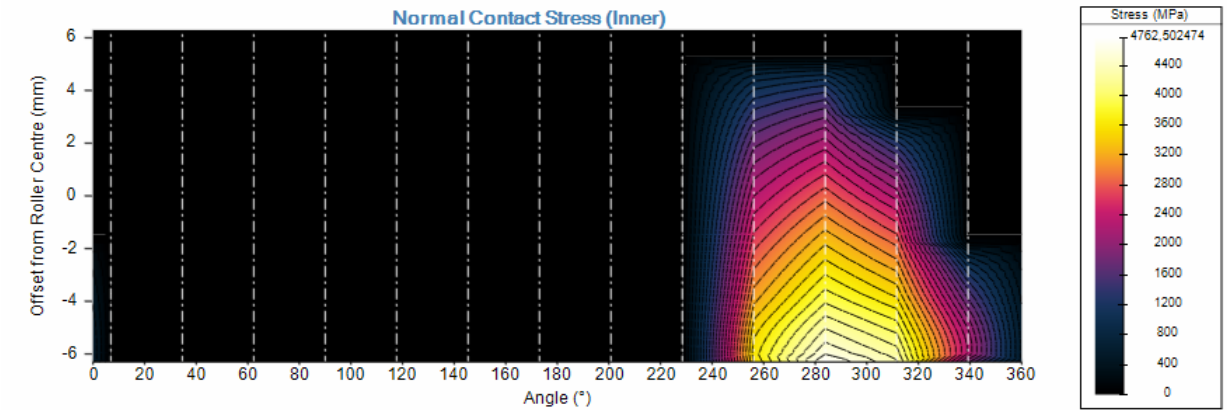

Figure 5.1: Highest loaded bearing element during abuse drive case. Significant edge loading could be observed.

5.3 Future work

To move forward with the gearbox design, tolerances for all components need to be set and tolerance stackup analysis conducted to ensure that the entire system is within tolerance. E.g. is the distance between the axial bearing surfaces on the planet carrier, where bearing clearance needs to be sufficient for the planet shafts to rotate without excessive friction but with limited side-to-side play. Tolerances for bearing seats and surface finish at rotating seals should also be considered.

The effect of transmission error could also be investigated further. The suggested superimposed torque resulting from the peak-to-peak TE could not be fully investigated in this master thesis due to time constraints. A simulation of the oscillations including component stiffness and inertia could reveal the true effect on the system. The significance of the effect on system torque could determine if TE should be a design consideration in this type of application.

Once a prototype of the gearbox is built a further gear oil evaluation should be performed. Required oil level, efficiency losses and operating temperature are difficult to simulate and should be tested with representable driving cycles. Gear oils with different viscosity grades could be tested to evaluate the performance and trade-offs in efficiency and protection of the gears. Oil level should be investigated in order to establish a level that ensures proper lubrication of all parts but does not add unnecessary drag losses from the fluid. To ensure that oil reaches all critical parts of the gearbox a fluorescent additive can be included in the oil and test cycles of different speeds could be run. After each test cycle the gearbox is dismantled and inspected to see where oil is present. Operating temperature should be tested by simulating an endurance event to make sure the oil is within a proper operating temperature during the entire event. Knowledge of the operating temperature will help selecting an oil with proper viscosity. Efficiency losses are interesting both in the selection of oil level but also in which oil to use. The oil with the least efficiency losses while still achieving proper protection of the gears should be selected.

To further improve the gearset and potentially reduce additional weight, asymmetrical teeth profiles could be considered. To simplify the design process no helix angle was included and the tooth flank modifications were mirrored across each tooth. Since the gear loads are different during driving and regenerative braking as well as different between the front and rear wheels the tooth design could be optimized for the specific use case. For a rear wheel gearbox the driving loads will be high while loads during regenerative braking will be lower due to weight transfer and tire grip level. Therefore the gear teeth could be optimized for heavier loads on one of the flanks reducing both bending and contact stress. This design approach could result in four different gearset designs as each wheel would require a unique gearbox optimized for the use case. A greater number of unique parts increase cost and spare parts are not interchangeable, further increasing number of components that have to be produced. The approach would also require more data on torque levels and the use case that each wheel experiences. Since no previous data of an AWD system was available to Lund Formula Student and the cost of implementation had to be kept reasonable a more conservative design approach was used.

Another approach to improve the gearset would be to use optimization algorithms to find optimal values for the design parameters. Multiple methods of optimisation of gearsets have been presented in recent research with positive results. The challenge with using optimization algorithms is however to define the limits of design space. As the complexity of a transmission system is increased each design parameter start to influence other parts of the design which have to be accounted for in the algorithm. The potential for increased safety factors and possible size reduction is however interesting and could be investigated.

Bibliography

[1] Ken Mao. *The Conceptualisation, Development, Design and Optimisation of an Integrated In-Hub Planetary Gearbox System for a Formula Student Race Car*. Master of Engineering in Automotive Engineering 3rd Year Dissertation. School of Engineering at the University of Warwick, 2022.

[2] Peder August Aune. *a Four Wheel Drive System for a Formula Style Electric Racecar*. Master Thesis. Norwegian University of Science and Technology - Department of Product Design, 2016.

[3] Formula Student Germany. *FS-Rules 2024 v1.1*. URL: https://www.formulastudent.de/fsg/rules/.

[4] Formula Student East. *Results 2023 - Formula Student East*. URL: https://fseast.eu/results-2023/.

[5] Johan Litzén and Ludvig Nilsson. *Design of a Compound Planetary Gearbox for a Formula Student Car*. Project course work. Lunds Tekniska Högskola, 2022.

[6] Lars Vedmar. *Maskinelement Transmissioner*. Lunds Tekniska Högskola, 2017.

[7] Daniel Miler and Matija Hoić. "Optimisation of cylindrical gear pairs: A review". In: *Mechanism and Machine Theory* 156 (2021), p. 104156. ISSN: 0094-114X. DOI: https://doi.org/10.1016/j.mechmachtheory.2020.104156. URL: https://www.sciencedirect.com/science/article/pii/S0094114X20303736.

[8] International Organization for Standardization. *Calculation of load capacity of spur and helical gears — Part 5: Strength and quality of materials*. ISO 6336-5:2016(E). Geneva, Switzerland: International Organization for Standardization, 2016.

[9] International Organization for Standardization. *Cylindrical gears — ISO system of flank tolerance classification — Part 1: Definitions and allowable values of deviations relevant to flanks of gear teeth*. ISO 1328-1:2013(E). Geneva, Switzerland: International Organization for Standardization, 2013.

[10] International Organization for Standardization. *Gears — Cylindrical involute gears and gear pairs — Concepts and geometry*. ISO 21771:2007(E). Geneva, Switzerland: International Organization for Standardization, 2007.

[11] Chanho Choi et al. "Influence of gear tooth addendum and dedendum on the helical gear optimization considering mass, efficiency, and transmission error". In: *Mechanism and Machine Theory* 166 (2021), p. 104476. ISSN: 0094-114X. DOI: https://doi.org/10.1016/j.mechmachtheory.2021.104476. URL: https://www.sciencedirect.com/science/article/pii/S0094114X21002342.

[12] Christopher G. Cooley and Robert G. Parker. "A Review of Planetary and Epicyclic Gear Dynamics and Vibrations Research". In: *Applied Mechanics Reviews* 66.4 (June 2014), p. 040804. ISSN: 0003-6900. DOI: 10.1115/1.4027812. eprint: https://asmedigitalcollection.asme.org/appliedmechanicsreviews/article-pdf/66/4/040804/6074266/amr_066_04_040804.pdf. URL: https://doi.org/10.1115/1.4027812.

[13] Giorgio Bonori, Marco Barbieri, and Francesco Pellicano. "Optimum profile modifications of spur gears by means of genetic algorithms". In: *Journal of Sound and Vibration* 313.3 (2008), pp. 603–616. ISSN: 0022-460X. DOI: https://doi.org/10.1016/j.jsv.2007.12.013. URL: https://www.sciencedirect.com/science/article/pii/S0022460X07009911.

[14] Shuting Li. "Effects of machining errors, assembly errors and tooth modifications on loading capacity, load-sharing ratio and transmission error of a pair of spur gears". In: *Mechanism and Machine Theory* 42.6 (2007), pp. 698–726. ISSN: 0094-114X. DOI: https://doi.org/10.1016/j.mechmachtheory.2006.06.002. URL: https://www.sciencedirect.com/science/article/pii/S0094114X06001133.

[15] Yulong Lei et al. "Research on vibration and noise reduction of electric bus gearbox based on multi-objective optimization". In: *Applied Acoustics* 158 (2020), p. 107037. ISSN: 0003-682X. DOI: https://doi.org/10.1016/j.apacoust.2019.107037. URL: https://www.sciencedirect.com/science/article/pii/S0003682X19301100.

[16] A. Dyson. "Scuffing - a review". In: *Tribology International* 8.2 (1975), pp. 77–87. ISSN: 0301-679X. DOI: https://doi.org/10.1016/0301-679X(75)90056-0. URL: https://www.sciencedirect.com/science/article/pii/0301679X75900560.

[17] International Organization for Standardization. *Calculation of load capacity of spur and helical gears — Part 20: Calculation of scuffing load capacity — Flash temperature method*. ISO 6336-20:2022(E). Geneva, Switzerland: International Organization for Standardization, 2022.

[18] International Organization for Standardization. *Calculation of load capacity of spur and helical gears — Part 20: Calculation of scuffing load capacity — Integral temperature method*. ISO 6336-21:2022(E). Geneva, Switzerland: International Organization for Standardization, 2022.

[19] Bernd-Robert Hoehn Peter Oster Thomas Tobie and Klaus Michaelis. "Test methods for gear lubricants". In: *goriva i maziva* 47,2 (2008), pp. 129–152. ISSN: 0350-350X. URL: https://hrcak.srce.hr/file/37724.

[20] Pan American Lubricants. *Useful information on scuffing load tests*. URL: https://www.panamlubricants.com/wp-content/uploads/2016/08/FZG-Testing-Information.pdf.

[21] International Organization for Standardization. *Rolling bearings - Methods for calculating the modified reference rating life for universally loaded bearings*. ISO 16281:2008. Geneva, Switzerland: International Organization for Standardization, 2008.

[22] International Organization for Standardization. *Rolling bearings – Dynamic load ratings and rating life (ISO 281:2007, IDT)*. ISO 281:2007. Geneva, Switzerland: International Organization for Standardization, 2007.

[23] Hanjun Gao et al. "Fatigue life of 7075-T651 aluminium alloy treated with vibratory stress relief". In: *International Journal of Fatigue* 108 (2018), pp. 62–67. ISSN: 0142-1123. DOI: https://doi.org/10.1016/j.ijfatigue.2017.11.011. URL: https://www.sciencedirect.com/science/article/pii/S0142112317304371.

[24] Takayuki Shiraiwa, Fabien Briffod, and Manabu Enoki. "Prediction of Fatigue Crack Initiation of 7075 Aluminum Alloy by Crystal Plasticity Simulation". In: *Materials* 16.4 (2023). ISSN: 1996-1944. DOI: 10.3390/ma16041595. URL: https://www.mdpi.com/1996-1944/16/4/1595.

[25] Tianwen Zhao and Yanyao Jiang. "Fatigue of 7075-T651 aluminum alloy". In: *International Journal of Fatigue* 30.5 (2008), pp. 834–849. ISSN: 0142-1123. DOI: https://doi.org/10.1016/j.ijfatigue.2007.07.005. URL: https://www.sciencedirect.com/science/article/pii/S014211230700196X.

[26] International Organization for Standardization. *Calculation of load capacity of spur and helical gears — Part 3: Calculation of tooth bending strength*. ISO 6336-3:2019(E). Geneva, Switzerland: International Organization for Standardization, 2019.

[27] Franco Concli. "Tooth Root Bending Strength of Gears: Dimensional Effect for Small Gears Having a Module below 5 mm". In: *Applied Sciences* 11.5 (2021). ISSN: 2076-3417. DOI: 10.3390/app11052416. URL: https://www.mdpi.com/2076-3417/11/5/2416.

[28] P. Hoehn B.R. Oster and C Braykoff. "Size and material influence on the tooth root, pitting, scuffing and wear load carrying capacity of fine module gears." In: *Gear Technology* (2011). URL: https://www.geartechnology.com/articles/20740-size-and-material-influence-on-the-tooth-root-pitting-scuffing-and-wear-load-carrying-capacity-of-fine-module-gears.

[29] Bodycote. *Ytbehandling Tuframm*. Data sheet.

Appendix A

Appendix

A.1 Planet carrier

A.1.1 Aluminium 7075 fatigue properties

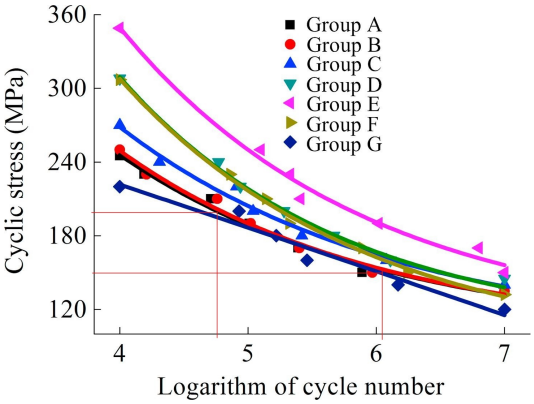

Figure A.1: Aluminium 7075 S-N curve from Gao et. al.

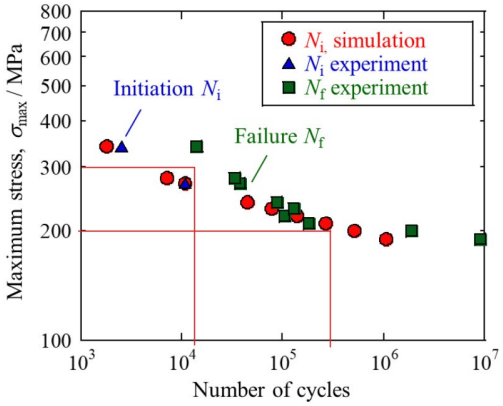

Figure A.2: Aluminium 7075 S-N curve from Shiraiwa et. al.

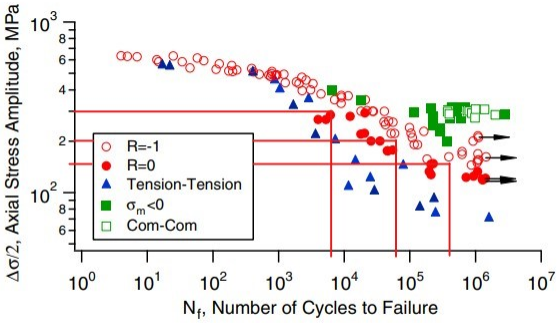

Fig. 8. Stress–life of all the uniaxial fatigue experiments conducted.

Figure A.3: Aluminium 7075 S-N curve from Zhao et. al.

A.1.2 Load cases for planet carrier analysis

FEA was conducted on the planet carrier with the following load cases. The FEA results are not however included in this report.

Wheel loads

Abuse wheel force load case was used to dimension the planet carrier as a worst case scenario. Stress levels were keept below material yield stress for this load case.

Wheel nut tightening torque

To analyse the necessary wheel nut tightening torque and requirement of drive pegs on the hub, the wheel nut preload was calculated using:

$$T = F_p(\frac{P}{2\pi} + \frac{\mu_t * r_t}{cos\beta} + \mu_n * r_n)$$

Where:
T - Tightening torque
F_p - Fastener preload
P - Thread pitch
μ_t - Coefficient of friction in threads
r_t - Half thread pitch diameter
β - Half angle of thread form
μ_n - Coefficient of friction under nut head
r_n - Effective radius of head contact

Since the wheel nut contact surface was conical with an angle of 90°the equation became:

$$T = F_p(\frac{P}{2\pi} + \frac{\mu_t * r_t}{cos\beta} + \frac{\mu_n * r_n}{sin(45°)})$$

As the threads of the wheel nut and threads on the planet carrier will be anodized the thread coefficient of friction was assumed to be 0.11 according to Bodycote's anodizing Tufram [29]. The friction between anodized wheel nut and the magnesium wheel was assumed to be 0.15. Using the above equation a tightening torque of **325 Nm** resulted in a fastener preload of about **35 kN** which was used in the structural analysis.

Table A.1: Wheel nut tightening torque parameters

Parameter	**Symbol**	**Value**
Tightening torque	T	325 Nm
Thread pitch	P	1,5 mm
Coefficient of friction in threads	μ_t	0,11
Half thread pitch diameter	r_t	24 mm
Half angle of thread form	β	30°
Coefficient of friction under nut head	μ_t	0,15
Effective radius of head contact	r_n	29 mm

Braking torque

The brake disc tabs on the planet carrier were analysed in order to ensure sufficient strength when braking from approximate vehicle top speed of 120 kph. Data from driving indicate that a coefficient of friction of 1.85 can occur and a wheel load distribution of 0.45 at a front wheel during hard braking.

Table A.2: Brake torque calculation

Parameter	**Value**
cl*A	4,5
Top speed	120 kph
Front downforce distribution	0,4
Wheel load distribution	0,45
Coefficient of friction	1,85
Loaded tire radius	0,194 m

The parameters resulted in a maximum braking torque of **673 Nm**.

A.2 Load cases

The fatigue, acceleration and abuse load case parameters used as input in MASTA are presented in the following tables.

Fatigue loads

Motor torque (Nm)	*Motor rpm*	*Duration (h)*	*Force Y (kN)*	*Axial Load (kN)*	*Mx (Nm)*	*My (Nm)*
-7,645326	8286,665677	0,048063	0,957511	-0,401427	56,811551	9,792180
-7,645326	8286,665677	0,124963	1,088572	0,175391	-57,974470	10,772306
-7,645326	8286,665677	0,115350	1,172233	0,972649	-214,482944	13,606270
-7,645326	8286,665677	0,144188	1,119301	1,400690	-296,358507	10,474128
-7,645326	8286,665677	0,009613	1,114546	1,930049	-398,949550	9,075393
-2,803886	7174,313391	2,393517	0,624244	-0,373814	58,786621	3,672184
-2,803886	7174,313391	0,701714	0,859551	0,158886	-49,734022	4,722804
-2,803886	7174,313391	0,374888	0,981283	0,811835	-179,084286	4,679395
-2,803886	7174,313391	0,692101	1,202440	1,437042	-305,239732	4,658944
-2,803886	7174,313391	0,086513	1,168210	1,842557	-383,156669	5,550740
0,267336	6548,705804	5,959762	0,292301	-0,243583	40,824422	-0,081026
0,267336	6548,705804	0,817064	0,613693	0,127023	-38,143786	-0,438115
0,267336	6548,705804	0,259538	1,013137	0,908382	-198,515112	-2,279270
0,267336	6548,705804	0,845902	1,155414	1,507990	-317,969120	-1,827664
0,267336	6548,705804	0,163413	1,195596	1,857986	-386,752395	-1,177812
4,354843	7185,187713	0,144188	0,446732	-0,136814	16,713754	-7,031262
4,354843	7185,187713	0,192250	0,626096	0,138785	-40,698477	-6,802447
4,354843	7185,187713	0,346051	1,070210	1,041372	-225,570869	-6,350924
4,354843	7185,187713	1,028540	1,157040	1,427676	-302,424011	-6,293287
4,354843	7185,187713	0,038450	1,082025	1,881570	-388,829115	-6,228004
7,366654	7575,336278	0,173025	0,435781	-0,103292	10,451481	-11,201488
7,366654	7575,336278	0,586364	0,643080	0,148029	-42,865410	-11,045328
7,366654	7575,336278	0,557526	0,974813	0,930557	-201,973934	-10,241044
7,366654	7575,336278	0,797839	1,138059	1,389226	-294,547063	-11,080642
7,366654	7575,336278	0,009613	1,091384	1,797472	-372,720055	-11,020657
10,102002	7316,093735	0,451788	0,513964	-0,150741	17,936623	-14,809299
10,102002	7316,093735	0,480626	0,660494	0,216016	-56,438059	-14,699972
10,102002	7316,093735	0,471013	0,918593	0,933789	-201,364077	-15,091542
10,102002	7316,093735	0,355663	1,085340	1,321294	-280,208459	-14,995471
10,102002	7316,093735	0,000000	0,000000	0,000000	0,000000	0,000000
13,059603	7797,820779	0,297988	0,443373	-0,107184	11,039512	-19,004040
13,059603	7797,820779	0,653651	0,647218	0,159873	-45,254059	-19,547791
13,059603	7797,820779	0,769002	0,904954	0,849527	-184,717312	-19,349560
13,059603	7797,820779	0,346051	1,102329	1,269312	-270,497756	-18,694883
13,059603	7797,820779	0,000000	0,000000	0,000000	0,000000	0,000000
15,732975	8503,865369	0,297988	0,428500	-0,085048	7,072314	-22,651420
15,732975	8503,865369	0,730551	0,618363	0,199603	-52,326982	-23,294619
15,732975	8503,865369	0,711326	0,963038	0,851339	-186,346694	-23,255473
15,732975	8503,865369	0,067288	0,988040	1,261983	-266,561517	-23,853855
15,732975	8503,865369	0,000000	0,000000	0,000000	0,000000	0,000000
18,549991	7423,871979	0,000000	0,000000	0,000000	0,000000	0,000000
18,549991	7423,871979	0,153800	0,650245	0,293301	-71,205729	-26,887115
18,549991	7423,871979	0,221088	0,938242	0,840809	-183,758186	-27,308174
18,549991	7423,871979	0,096125	1,042933	1,385573	-291,745778	-28,171596
18,549991	7423,871979	0,000000	0,000000	0,000000	0,000000	0,000000
22,402000	8638,249634	0,000000	0,000000	0,000000	0,000000	0,000000

22,402000	8638,249634	0,038450	0,786776	0,454012	-105,387305	-32,463990
22,402000	8638,249634	0,028838	0,845852	0,884630	-190,226968	-33,774483
22,402000	8638,249634	0,000000	0,000000	0,000000	0,000000	0,000000
22,402000	8638,249634	0,000000	0,000000	0,000000	0,000000	0,000000
24,750613	8689,984831	0,000000	0,000000	0,000000	0,000000	0,000000
24,750613	8689,984831	0,067288	0,688814	0,455175	-103,457896	-36,614474
24,750613	8689,984831	0,192250	0,794208	0,792971	-171,309049	-36,443758
24,750613	8689,984831	0,000000	0,000000	0,000000	0,000000	0,000000
24,750613	8689,984831	0,000000	0,000000	0,000000	0,000000	0,000000
28,352295	8179,265264	0,000000	0,000000	0,000000	0,000000	0,000000
28,352295	8179,265264	0,403726	0,634970	0,423078	-96,046438	-41,853209
28,352295	8179,265264	0,288376	0,736788	0,712193	-154,374854	-41,720018
28,352295	8179,265264	0,000000	0,000000	0,000000	0,000000	0,000000
28,352295	8179,265264	0,000000	0,000000	0,000000	0,000000	0,000000
0	0	0,005556	1,543113	0	33,948486	0

Acceleration loads		
Motor torque (Nm)	*Motor rpm*	*Duration (h)*
29	12000	0,1
27,8	14000	0,1
24,8	16000	0,1
21,4	18000	0,1
18	20000	0,1

Abuse drive				
Motor torque (Nm)	*Motor rpm*	*Force Y (kN)*	*Axial Load (kN)*	*Mx (Nm)*
46,4	10	0	0	0
Abuse regen				
Motor torque (Nm)	*Motor rpm*	*Force Y (kN)*	*Axial Load (kN)*	*Mx (Nm)*
-46,4	10	0	0	0
Abuse wheel force				
Motor torque (Nm)	*Motor rpm*	*Force Y (kN)*	*Axial Load (kN)*	*Mx (Nm)*
3,4829	6997,8157	3,289917	2,302000	-518,966172

A.3 Gearset

A.3.1 Gearset efficiency

The theoretical gearbox efficiency was calculated using the following formula:

$$\eta = \frac{1 - \eta_k^2 R}{1 - R}$$

Where η_k is the gear efficiency (assumed to be 0.99) and R is the fixed carrier ratio.

A.3.2 Geometry reports from MASTA

SMT

MASTA

Input stage

Cylindrical Planetary Gear Set Design

Gears

Name				Sun	Planet
Number of Teeth			z	18	47
Normal Module (mm)			m_n	1	
Flank Name				Both Flanks	
Normal Pressure Angle (°)			α_n	20	
Helix Angle (°)			β	0	
Helix Angle (Maintain Transverse Profile) (°)			β	0	
Transverse Pressure Angle (°)			α_t	20	
Material Name				Default Material	Default Material
Reference Diameter (mm)			d	18	47
Profile Shift Coefficient	Nominal (Zero Backlash)		x	0,13 (Specified)	-0,13 (Calculated from Sun)
	Average (Mean) Metal		x_E	0,1506 (Calculated)	-0,338 (Calculated)
Flank Name				Both Flanks	Both Flanks
Tip Diameter (mm)			d_a	20,46 (From Basic Rack)	48,54 (From Basic Rack)
Tip Form Diameter (mm)			d_{Fa}	20,26	48,34
Root Diameter (mm)			d_f	15,48 (From Basic Rack)	44,14 (From Basic Rack)
Rim Diameter (mm)				0	13
Base Diameter (mm)			d_b	16,914	44,166
Normal Base Pitch (mm)			p_{bn}	2,952	2,952
Normal Thickness	Average (Mean) Metal (mm)		$s_{n\ average}$	1,68 (Calculated)	1,325 (Calculated)
Mean Normal Thickness At Tip Form Diameter (mm)			$s_{n\ Fa}$	0,645	0,812
Tip Thickness (mm)				0,439	0,609
Face Width (mm)			b	14	13
Root Form Diameter (mm)			d_{Ff}	16,917	45,249
Lowest Start of Active Profile	Diameter (mm)			17,11	45,534
Basic Rack Addendum Factor			h_{aP}*	1,1 (Specified)	0,9 (Specified)
Basic Rack Dedendum Factor			h_{fP}*	1,39 (Specified)	1,3 (Specified)
Residual Fillet Undercut (mm)			s_{pr}	0	0
Normal Thickness	Maximum Metal (mm)		$s_{n\ max}$	1,695 (Calculated)	1,34 (Calculated)
	Minimum Metal (mm)		$s_{n\ min}$	1,665 (Calculated)	1,31 (Calculated)
	Tolerance (mm)		T_{sn}	0,03 (Specified)	0,03 (Specified)
Over Balls	Maximum Metal (mm)		$M_{dK\ upper}$	21,499 (Calculated)	49,267 (Calculated)
	Minimum Metal (mm)		$M_{dK\ lower}$	21,442 (Calculated)	49,189 (Calculated)
Ball Diameter (mm)			D_M	2 (From Form Diameters)	1,85 (From Form Diameters)
Chordal Span	Maximum Metal (mm)		$W_{k\ upper}$	4,797 (Calculated)	13,726 (Calculated)
	Minimum Metal (mm)		$W_{k\ lower}$	4,769 (Calculated)	13,698 (Calculated)

Gears

Number of Teeth For Chordal Span Test		k	2 (From Number of Teeth)	5 (From Number of Teeth)
Profile Quality Grade (ISO)			7	7
Helix Quality Grade (ISO)			7	7
Pitch Quality Grade (ISO)			7	7
Radial Quality Grade (ISO)			7	7

Materials

Name			Sun	Planet
Quality Grade			MQ	MQ
Material Has A Well Defined Yield Point?			Yes	Yes
Use ISO 6336-5 (2003) Material Definitions?			No	No
Limited Pitting Allowed?			No	No
Long Life Life Factor Bending			0,85	0,85
Long Life Life Factor Contact			0,85	0,85
N-0 (Contact) ($\times 10^6$)			0,1	0,1
N-0 (Bending) ($\times 10^6$)			0,001	0,001
Material Type			Case Hardening (Carburized) Steel, Core Hardness >= 25 HRC, Jominy Hardenability at J=12mm >= HRC 28	Case Hardening (Carburized) Steel, Core Hardness >= 25 HRC, Jominy Hardenability at J=12mm >= HRC 28
Modulus Of Elasticity (MPa)		E	207000	207000
Use Custom Material for Contact?			No	No
Use Custom Material for Bending?			No	No
Allowable Stress Number (Bending) (MPa)		σ_{FE}	920	920
Retained Austenite (%)			0	0
Shot Peened?			No	No
Specify Allowable Stress Number (Bending)?			No	No
Specify Allowable Stress Number (Contact)?			No	No
Nominal Stress Number (Bending) (MPa)		$\sigma_{F\ lim}$	460	460
Allowable Stress Number (Contact) (MPa)		$\sigma_{H\ lim}$	1500	1500
N-C (Contact) ($\times 10^6$)			50	50
N-C (Bending) ($\times 10^6$)			3	3
Core Hardness			316,8571	316,8571
Material Name			Default Material	Default Material
Density (kg/m^3)		ρ	7800	7800
Poisson's Ratio		ν	0,3	0,3
Plane Strain Modulus (MPa)		E'	227472,5275	227472,5275
Coefficient Of Thermal Expansion (µm/(m·K))		α	12	12
Shear Modulus (MPa)		G	79615,3846	79615,3846
Shear Yield Stress (MPa)		τ_{yield}	361,25	361,25
Shear Fatigue Strength (MPa)		τ_a	216,75	216,75
Standard			Custom	Custom
Hardness Type			Vickers (HV)	Vickers (HV)
Surface Hardness			700	700
Surface Hardness Range Max in HRC			61,9577	61,9577
Surface Hardness Range Min in HRC			57,49	57,49

Materials

Surface Hardness Range Max in HB			687,2385	687,2385
Surface Hardness Range Min in HB			604,8	604,8
Surface Hardness Range Max in HV			744,9	744,9
Surface Hardness Range Min in HV			642,8	642,8
Tensile Yield Strength (MPa)		R_e	750	750
Ultimate Tensile Strength (MPa)		R_m	850	850
Heat Conductivity (N/(s·K))		k	45	45
Specific Heat (J/(kg·K))			500	500
History			History is not applicable for default database items	History is not applicable for default database items
Status				

Gear Accuracy

Name			Sun	Planet
Tolerance Standard			ISO 1328-1:1995(E)/ISO 1328-2:1997(E)	ISO 1328-1:1995(E)/ISO 1328-2:1997(E)
Profile Form Deviation	**(µm)**		7 (Calculated according to ISO 1328-1:1995(E))	8 (Calculated according to ISO 1328-1:1995(E))
Profile Slope Deviation			6 (Calculated according to ISO 1328-1:1995(E))	6,5 (Calculated according to ISO 1328-1:1995(E))
Total Profile Deviation			9 (Calculated according to ISO 1328-1:1995(E))	10 (Calculated according to ISO 1328-1:1995(E))
Helix Form Deviation			10 (Calculated according to ISO 1328-1:1995(E))	10 (Calculated according to ISO 1328-1:1995(E))
Helix Slope Deviation			10 (Calculated according to ISO 1328-1:1995(E))	10 (Calculated according to ISO 1328-1:1995(E))
Total Helix Deviation			14 (Calculated according to ISO 1328-1:1995(E))	14 (Calculated according to ISO 1328-1:1995(E))
Single Pitch Deviation			9,5 (Calculated according to ISO 1328-1:1995(E))	10 (Calculated according to ISO 1328-1:1995(E))
Cumulative Pitch Deviation			13 (Calculated according to ISO 1328-1:1995(E))	17 (Calculated according to ISO 1328-1:1995(E))
Total Cumulative Pitch Deviation			23 (Calculated according to ISO 1328-1:1995(E))	29 (Calculated according to ISO 1328-1:1995(E))
Number of Pitches for Sector Pitch Deviation			2	6
Total Radial Composite Deviation	**(µm)**		26 (Calculated according to ISO 1328-2:1997(E))	31 (Calculated according to ISO 1328-2:1997(E))
Tooth-to-Tooth Radial Composite Deviation			7,5 (Calculated according to ISO 1328-2:1997(E))	7,5 (Calculated according to ISO 1328-2:1997(E))
Runout			18 (Calculated according to ISO 1328-2:1997(E))	23 (Calculated according to ISO 1328-2:1997(E))

Mesh

Name				Sun to Planet	
				Sun	Planet
Flank Name				Both Flanks	
Has Hunting Ratio?				Yes	
Highest Common Factor of Teeth Numbers				1	
Centre Distance (mm)			a_w	32,5	
Effective Face Width (mm)			b_{eff}	13	
Working Transverse Pressure Angle (°)			α_{wt}	20	
Working Helix Angle (°)				0	
Working Pitch Diameter (mm)			d_w	18	47
Sum of Profile Shift Coefficient			Σ_x	0	
Profile Shift Coefficient	**Nominal (Zero Backlash)**		x	0,13 (Specified)	-0,13 (Calculated from Sun)
	Average (Mean) Metal		x_E	0,1506 (Calculated)	-0,338 (Calculated)
Total Contact Ratio			ε_γ	1,4518	
Transverse Contact Ratio			ε_α	1,4518	
Axial Contact Ratio			ε_β	0	
Flank Name				Left	

Mesh

Normal Backlash	**Minimum (mm)**			0,1 (Specified)	
	Maximum (mm)			0,156 (Calculated)	
Number of Teeth			z	18	47
Ratio			u	2,6111	
Normal Module (mm)			m_n	1	1
Flank Name				Both Flanks	Both Flanks
Sliding Factor At Tooth Tip			K_{ga}	0,3838	0,2748
Normal Pressure Angle (°)			α_n	20	20
Helix Angle (°)			β	0	0
Transverse Pressure Angle (°)			α_t	20	20
Reference Diameter (mm)			d	18	47
Tip Diameter (mm)			d_a	20,46 (From Basic Rack)	48,54 (From Basic Rack)
Tip Form Diameter (mm)			d_{Fa}	20,26	48,34
Root Diameter (mm)			d_f	15,48 (From Basic Rack)	44,14 (From Basic Rack)
Base Diameter (mm)			d_b	16,914	44,166
Normal Base Pitch (mm)			p_{bn}	2,952	2,952
Mean Normal Thickness At Tip Form Diameter (mm)			$s_{n\,Fa}$	0,645	0,812
Face Width (mm)			b	14	13
Root Form Diameter (mm)			d_{Ff}	16,917	45,249
Start of Active Profile	**Rolling Distance (mm)**			1,29	5,54
	Diameter (mm)			17,11	45,534
Highest Point of Fewest Tooth Contacts	**Rolling Distance (mm)**			4,242	8,492
Lowest Point of Fewest Tooth Contacts				2,624	6,873
Basic Rack Addendum Factor			h_{aP}*	1,1 (Specified)	0,9 (Specified)
Basic Rack Dedendum Factor			h_{fP}*	1,39 (Specified)	1,3 (Specified)

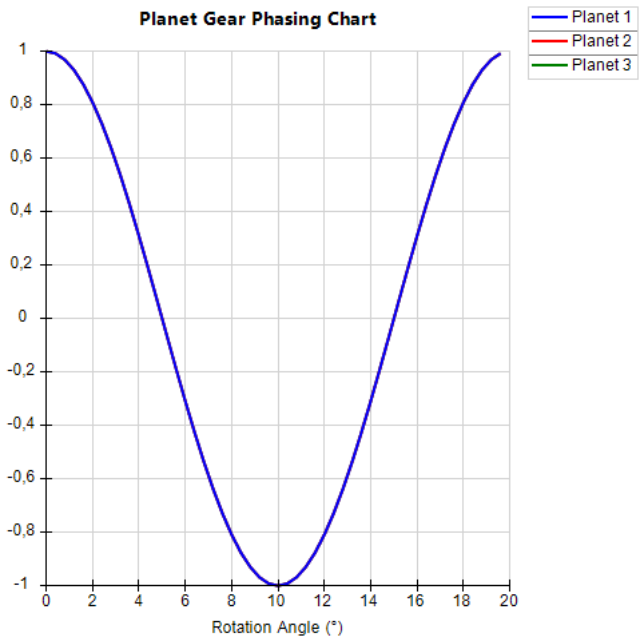

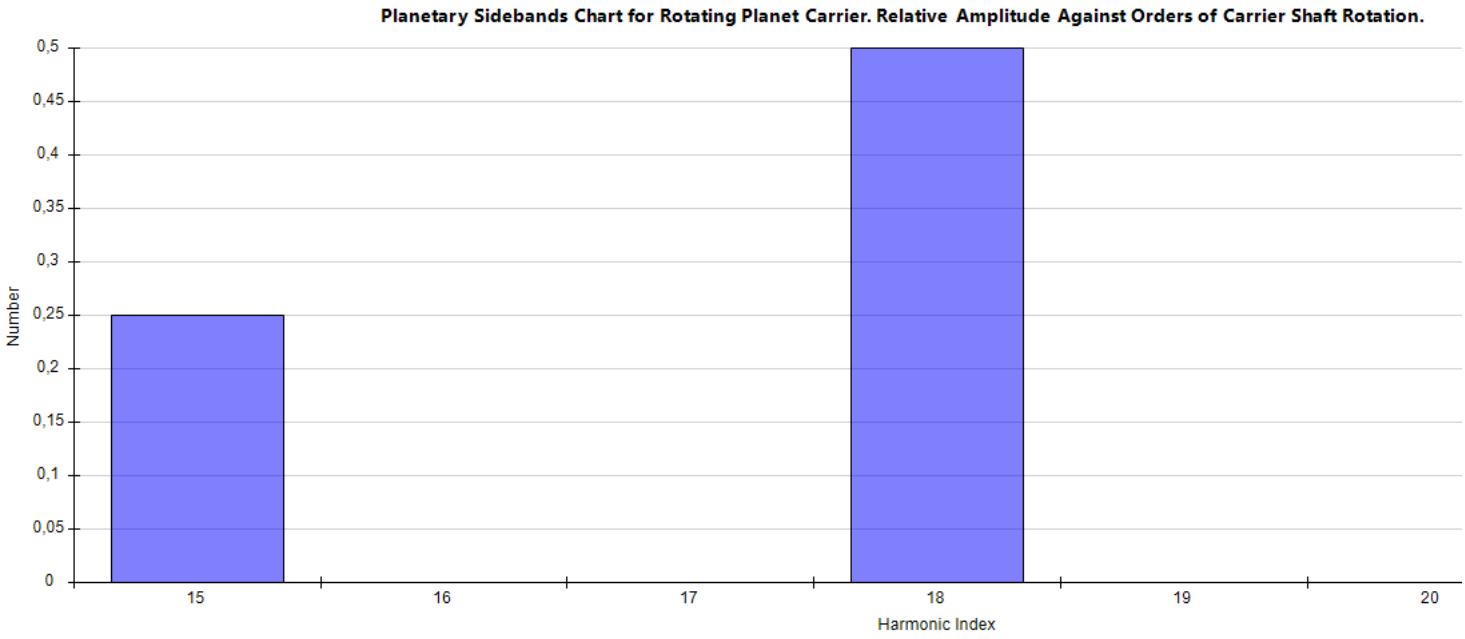

C:\Users\jlitzen\OneDrive - BorgWarner\Exjobb\MASTA\LFS Planetary gearbox_6_v12.Masta
Hash Code: 5d6b934a
MASTA 13.0.1 Build 161265+3afa346d88d5 (RLM) 2024-04-09 17:42:24

SMT

MASTA

Output stage

Cylindrical Planetary Gear Set Design

Gears

Name				Planet	Annulus
Number of Teeth			z	19	84
Normal Module (mm)			m_n	1	
Flank Name				Both Flanks	
Normal Pressure Angle (°)			α_n	20	
Helix Angle (°)			β	0	
Helix Angle (Maintain Transverse Profile) (°)			β	0	
Transverse Pressure Angle (°)			α_t	20	
Material Name				Default Material	Nitrided steel - default
Reference Diameter (mm)			d	19	-84
Profile Shift Coefficient	Nominal (Zero Backlash)		x	0,45 (Specified)	-0,45 (Calculated from Planet)
	Average (Mean) Metal		x_E	0,4706 (Calculated)	-0,5995 (Calculated)
Flank Name				Both Flanks	Both Flanks
Tip Diameter (mm)			d_a	21,7 (From Basic Rack)	83,03 (From Basic Rack)
Tip Form Diameter (mm)			d_{Fa}	21,5	-83,23
Root Diameter (mm)			d_f	17,14 (From Basic Rack)	87,5 (From Basic Rack)
Rim Diameter (mm)				13	-95
Base Diameter (mm)			d_b	17,854	-78,934
Normal Base Pitch (mm)			p_{bn}	2,952	2,952
Normal Thickness	Average (Mean) Metal (mm)		$s_{n\ average}$	1,913 (Calculated)	1,134 (Calculated)
Mean Normal Thickness At Tip Form Diameter (mm)			$s_{n\ Fa}$	0,766	0,856
Tip Thickness (mm)				0,56	0,658
Face Width (mm)			b	14	15
Root Form Diameter (mm)			d_{Ff}	18,039	-87,1
Lowest Start of Active Profile	Diameter (mm)			18,333	86,028
Basic Rack Addendum Factor			h_{aP}*	0,9 (Specified)	0,9352 (Specified)
Basic Rack Dedendum Factor			h_{fP}*	1,38 (Specified)	1,3 (Specified)
Residual Fillet Undercut (mm)			s_{pr}	0	-
Normal Thickness	Maximum Metal (mm)		$s_{n\ max}$	1,928 (Calculated)	1,149 (Calculated)
	Minimum Metal (mm)		$s_{n\ min}$	1,898 (Calculated)	1,119 (Calculated)
	Tolerance (mm)		T_{sn}	0,03 (Specified)	0,03 (Specified)
Over Balls	Maximum Metal (mm)		$M_{dK\ upper}$	22,428 (Calculated)	82,792 (Calculated)
	Minimum Metal (mm)		$M_{dK\ lower}$	22,372 (Calculated)	82,871 (Calculated)
Ball Diameter (mm)			D_M	1,85 (From Form Diameters)	1,7 (From Form Diameters)
Chordal Span	Maximum Metal (mm)		$W_{k\ upper}$	7,982 (Calculated)	26,666 (Calculated)
	Minimum Metal (mm)		$W_{k\ lower}$	7,954 (Calculated)	26,694 (Calculated)

Gears

Number of Teeth For Chordal Span Test		k	3 (From Number of Teeth)	9 (From Number of Teeth)
Profile Quality Grade (ISO)			7	7
Helix Quality Grade (ISO)			7	7
Pitch Quality Grade (ISO)			7	7
Radial Quality Grade (ISO)			7	7

Materials

Name			Planet	Annulus
Quality Grade			MQ	MQ
Material Has A Well Defined Yield Point?			Yes	Yes
Use ISO 6336-5 (2003) Material Definitions?			No	Yes
Limited Pitting Allowed?			No	No
Long Life Life Factor Bending			0,85	0,85
Long Life Life Factor Contact			0,85	0,85
N-0 (Contact) ($\times 10^6$)			0,1	0,1
N-0 (Bending) ($\times 10^6$)			0,001	0,001
Material Type			Case Hardening (Carburized) Steel, Core Hardness >= 25 HRC, Jominy Hardenability at J=12mm >= HRC 28	Nitrided steel [NT(nitr)]
Modulus Of Elasticity (MPa)		E	207000	206000
Use Custom Material for Contact?			No	No
Use Custom Material for Bending?			No	No
Allowable Stress Number (Bending) (MPa)		σ_{FE}	920	840
Retained Austenite (%)			0	0
Shot Peened?			No	No
Specify Allowable Stress Number (Bending)?			No	No
Specify Allowable Stress Number (Contact)?			No	No
Nominal Stress Number (Bending) (MPa)		$\sigma_{F\ lim}$	460	420
Allowable Stress Number (Contact) (MPa)		$\sigma_{H\ lim}$	1500	1250
N-C (Contact) ($\times 10^6$)			50	2
N-C (Bending) ($\times 10^6$)			3	3
Core Hardness			316,8571	316,8571
Material Name			Default Material	Nitrided steel - default
Density (kg/m^3)		ρ	7800	7800
Poisson's Ratio		ν	0,3	0,3
Plane Strain Modulus (MPa)		E'	227472,5275	226373,6264
Coefficient Of Thermal Expansion (µm/(m·K))		α	12	12
Shear Modulus (MPa)		G	79615,3846	79230,7692
Shear Yield Stress (MPa)		τ_{yield}	361,25	510
Shear Fatigue Strength (MPa)		τ_a	216,75	306
Standard			Custom	Custom
Hardness Type			Vickers (HV)	Vickers (HV)
Surface Hardness			700	700
Surface Hardness Range Max in HRC			61,9577	Unknown
Surface Hardness Range Min in HRC			57,49	57,85
Surface Hardness Range Max in HB			687,2385	Unknown
Surface Hardness Range Min in HB			604,8	612
Surface Hardness Range Max in HV			744,9	900
Surface Hardness Range Min in HV			642,8	650
Tensile Yield Strength (MPa)		R_e	750	1200

Materials

Ultimate Tensile Strength (MPa)		R_m	850	1200
Heat Conductivity (N/(s·K))		k	45	45
Specific Heat (J/(kg·K))			500	500
Comment			-	
History			History is not applicable for default database items	-
Status				

Gear Accuracy

Name			Planet	Annulus
Tolerance Standard			ISO 1328-1:1995(E)/ISO 1328-2:1997(E)	ISO 1328-1:1995(E)/ISO 1328-2:1997(E)
Profile Form Deviation	**(µm)**		7 (Calculated according to ISO 1328-1:1995(E))	9 (Calculated according to ISO 1328-1:1995(E))
Profile Slope Deviation			6 (Calculated according to ISO 1328-1:1995(E))	7,5 (Calculated according to ISO 1328-1:1995(E))
Total Profile Deviation			9 (Calculated according to ISO 1328-1:1995(E))	12 (Calculated according to ISO 1328-1:1995(E))
Helix Form Deviation			10 (Calculated according to ISO 1328-1:1995(E))	11 (Calculated according to ISO 1328-1:1995(E))
Helix Slope Deviation			10 (Calculated according to ISO 1328-1:1995(E))	11 (Calculated according to ISO 1328-1:1995(E))
Total Helix Deviation			14 (Calculated according to ISO 1328-1:1995(E))	15 (Calculated according to ISO 1328-1:1995(E))
Single Pitch Deviation			9,5 (Calculated according to ISO 1328-1:1995(E))	11 (Calculated according to ISO 1328-1:1995(E))
Cumulative Pitch Deviation			13 (Calculated according to ISO 1328-1:1995(E))	20 (Calculated according to ISO 1328-1:1995(E))
Total Cumulative Pitch Deviation			23 (Calculated according to ISO 1328-1:1995(E))	37 (Calculated according to ISO 1328-1:1995(E))
Number of Pitches for Sector Pitch Deviation			2	10
Total Radial Composite Deviation	**(µm)**		26 (Calculated according to ISO 1328-2:1997(E))	37 (Calculated according to ISO 1328-2:1997(E))
Tooth-to-Tooth Radial Composite Deviation			7,5 (Calculated according to ISO 1328-2:1997(E))	7,5 (Calculated according to ISO 1328-2:1997(E))
Runout			18 (Calculated according to ISO 1328-2:1997(E))	29 (Calculated according to ISO 1328-2:1997(E))

Mesh

Name				Planet to Annulus	
				Planet	Annulus
Flank Name				Both Flanks	
Has Hunting Ratio?				Yes	
Highest Common Factor of Teeth Numbers				1	
Centre Distance (mm)			a_w	32,5	
Effective Face Width (mm)			b_{eff}	14	
Working Transverse Pressure Angle (°)			α_{wt}	20	
Working Helix Angle (°)				0	
Working Pitch Diameter (mm)			d_w	19	-84
Sum of Profile Shift Coefficient			Σ_x	0	
Profile Shift Coefficient	**Nominal (Zero Backlash)**		x	0,45 (Specified)	-0,45 (Calculated from Planet)
	Average (Mean) Metal		x_E	0,4706 (Calculated)	-0,5995 (Calculated)
Total Contact Ratio			ε_γ	1,324	
Transverse Contact Ratio			ε_α	1,324	
Axial Contact Ratio			ε_β	0	
Flank Name				Left	
Normal Backlash	**Minimum (mm)**			0,06 (Specified)	
	Maximum (mm)			0,116 (Calculated)	
Number of Teeth			z	19	84
Ratio			u	4,4211	
Normal Module (mm)			m_n	1	1
Flank Name				Both Flanks	Both Flanks
Sliding Factor At Tooth Tip			K_{ga}	0,2232	0,0952

Mesh

Helix Angle (°)			β	0	0
Transverse Pressure Angle (°)			α_t	20	20
Reference Diameter (mm)			d	19	-84
Tip Diameter (mm)			d_a	21,7 (From Basic Rack)	83,03 (From Basic Rack)
Tip Form Diameter (mm)			d_{Fa}	21,5	-83,23
Root Diameter (mm)			d_f	17,14 (From Basic Rack)	87,5 (From Basic Rack)
Base Diameter (mm)			d_b	17,854	-78,934
Normal Base Pitch (mm)			p_{bn}	2,952	2,952
Mean Normal Thickness At Tip Form Diameter (mm)			$s_{n\ Fa}$	0,766	0,856
Face Width (mm)			b	14	15
Root Form Diameter (mm)			d_{Ff}	18,039	-87,1
Start of Active Profile	**Rolling Distance (mm)**			2,08	17,105
	Diameter (mm)			18,333	86,028
Highest Point of Fewest Tooth Contacts	**Rolling Distance (mm)**			5,033	14,153
Lowest Point of Fewest Tooth Contacts				3,037	16,148
Basic Rack Addendum Factor			h_{aP}^*	0,9 (Specified)	0,9352 (Specified)
Basic Rack Dedendum Factor			h_{fP}^*	1,38 (Specified)	1,3 (Specified)

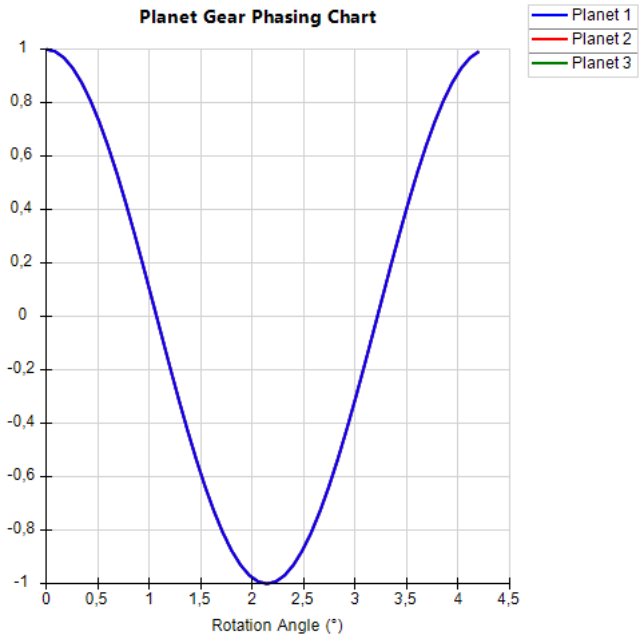

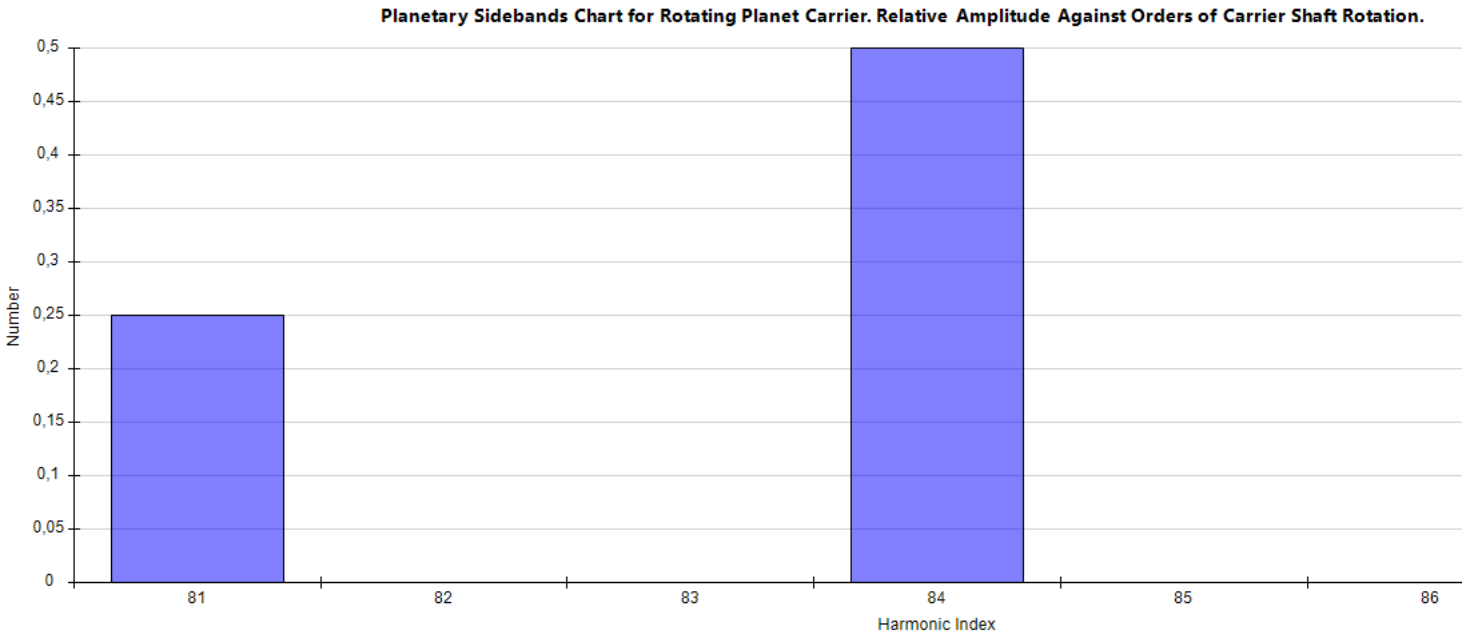

C:\Users\jlitzen\OneDrive - BorgWarner\Exjobb\MASTA\LFS Planetary gearbox_6_v12.Masta
Hash Code: 5d6b934a
MASTA 13.0.1 Build 161265+3afa346d88d5 (RLM) 2024-04-09 17:42:51

Micro Geometry Overview

Mesh Micro Geometry

Micro Geometry

Measured Micro Geometry

Mesh Micro Geometry

Name	Micro Geometry 4
	Sun to Planet

Micro Geometry

Name		Sun	Planet
Use Same Micro Geometry on Both Flanks?		No	No

Measured Micro Geometry

Name		Sun		Planet	
		Left Flank	Right Flank	Left Flank	Right Flank
Read Micro Geometry from an External File		Click To Open	Click To Open	Click To Open	Click To Open
Use Measured Map Data?		No	No	No	No

Central

Left Side

Right Side

Measured Micro Geometry

Meshed Gear Information

Left Flank Lead Modification Chart

Right Flank Lead Modification Chart

Central

Name		Sun		Planet	
		Left Flank	Right Flank	Left Flank	Right Flank
Crowning Relief (µm)		3	3	3	3
Linear Relief (ISO/DIN/AGMA/VDI) (µm)		-3	3	-3	3
Evaluation Left Limit (mm)		0	0	0	0
Evaluation Right Limit (mm)		14	14	13	13

Meshed Gear Information

Effective Face Width (mm)	b_{eff}	13

Left Side

Name	Sun		Planet	
	Left Flank	Right Flank	Left Flank	Right Flank
Linear Left Relief (µm)	0	0	0	0
Start Of Linear Left Relief (mm)	1,4	1,4	1,3	1,3
Evaluation Of Linear Left Relief (mm)	0	0	0	0
Parabolic Left Relief (µm)	0	0	0	0
Start Of Parabolic Left Relief (mm)	1,4	1,4	1,3	1,3
Evaluation Of Parabolic Left Relief (mm)	0	0	0	0

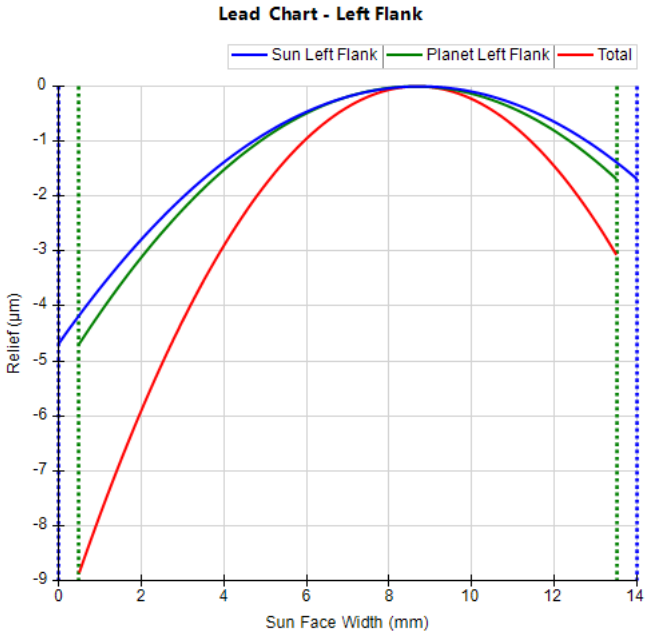

Right Side

Name	Sun		Planet	
	Left Flank	Right Flank	Left Flank	Right Flank
Linear Right Relief (µm)	0	0	0	0
Start Of Linear Right Relief (mm)	12,6	12,6	11,7	11,7
Evaluation Of Linear Right Relief (mm)	14	14	13	13
Parabolic Right Relief (µm)	0	0	0	0
Start Of Parabolic Right Relief (mm)	12,6	12,6	11,7	11,7
Evaluation Of Parabolic Right Relief (mm)	14	14	13	13

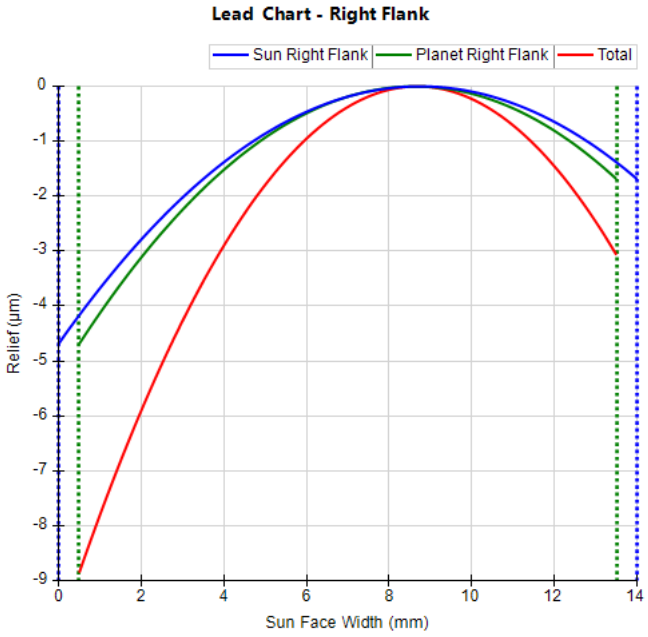

Measured Micro Geometry

Name	Sun		Planet	
	Left Flank	Right Flank	Left Flank	Right Flank
Use Measured Data?	No	No	No	No

Main Profile

Name		Sun		Planet	
		Left Flank	Right Flank	Left Flank	Right Flank
Barrelling Relief (µm)		5	5	5	5
Linear Relief (ISO/AGMA/DIN) (µm)		3	3	3	3
Location of Evaluation Upper Limit		User-Specified	User-Specified	User-Specified	User-Specified
Location of Evaluation Lower Limit		User-Specified	User-Specified	User-Specified	User-Specified
Evaluation Upper Limit	Rolling Distance (mm)	5,576	5,576	9,825	9,825
Evaluation Lower Limit		0,141	0,141	4,922	4,922
Main Profile Modification Ends at the Start of Tip Relief?		No	No	No	No
Main Profile Modification Ends at the Start of Root Relief?		No	No	No	No

Tip

Name		Sun		Planet	
		Left Flank	Right Flank	Left Flank	Right Flank
Location of Tip Relief Start		User-Specified	User-Specified	User-Specified	User-Specified
Location of Tip Relief Evaluation		Tip Form	Tip Form	Tip Form	Tip Form
Linear Tip Relief (µm)		0	0	0	0
Linear Tip Relief Start	Rolling Distance (mm)	5,033	5,033	9,335	9,335
Linear Tip Relief Evaluation		5,576	5,576	9,825	9,825
Parabolic Tip Relief (µm)		0	0	0	0
Parabolic Tip Relief Evaluation	Rolling Distance (mm)	5,576	5,576	9,825	9,825
Parabolic Tip Relief Start		5,033	5,033	9,335	9,335

Root

Name		Sun		Planet	
		Left Flank	Right Flank	Left Flank	Right Flank
Location of Root Modification Start		User-Specified	User-Specified	User-Specified	User-Specified
Location of Root Relief Evaluation		Root Form	Root Form	Root Form	Root Form
Linear Root Relief (µm)		0	0	0	0
Linear Root Relief Start	Rolling Distance (mm)	0,685	0,685	5,413	5,413
Linear Root Relief Evaluation		0,141	0,141	4,922	4,922
Parabolic Root Relief (µm)		0	0	0	0
Parabolic Root Relief Evaluation	Rolling Distance (mm)	0,141	0,141	4,922	4,922
Parabolic Root Relief Start		0,685	0,685	5,413	5,413

Meshed Gear Information

Profile Measured As			Roll Distance	
Flank Name			Both Flanks	
Length of Contact (mm)			4,286	
Name			Sun	Planet
Flank Name			Both Flanks	Both Flanks
Tip Form	Rolling Distance (mm)		5,576	9,825
End of Active Profile			5,576	9,825
Start of Active Profile			1,29	5,54
Root Form			0,141	4,922

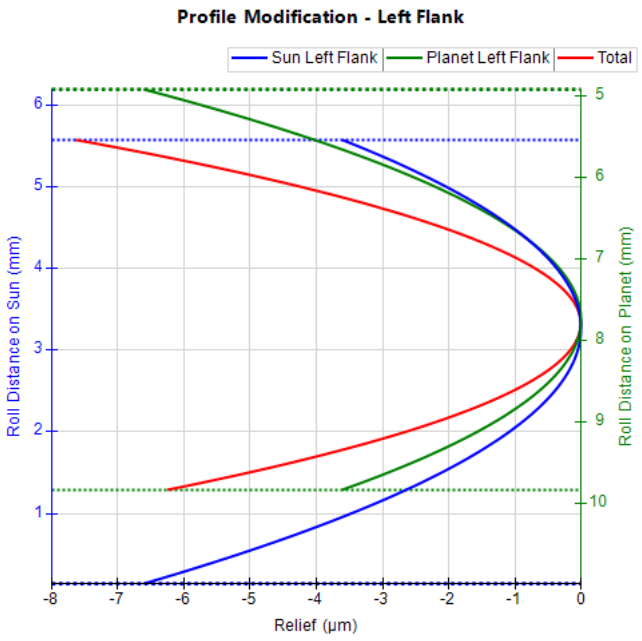

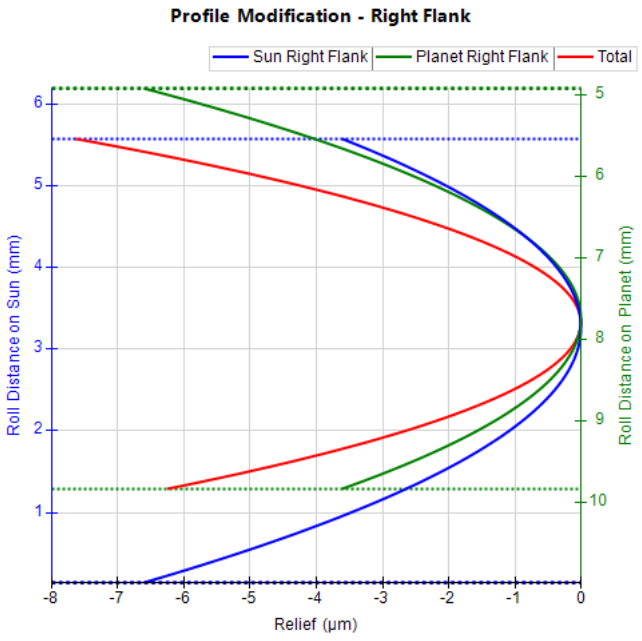

Measured Micro Geometry

Name	Sun		Planet	
	Left Flank	Right Flank	Left Flank	Right Flank
Use Measured Data?	No	No	No	No

Tip Left

Name			Sun		Planet	
			Left Flank	Right Flank	Left Flank	Right Flank
Linear	**Relief (µm)**		0	0	0	0
	Angle (°)		0 (Calculated)	0 (Calculated)	0 (Calculated)	0 (Calculated)
	Profile Evaluation	**Rolling Distance (mm)**	5,576	5,576	9,825	9,825
	Profile Start		5,033	5,033	9,335	9,335
	Face Width Position (mm)		0	0	0	0
Parabolic	**Relief (µm)**		0	0	0	0
	Angle (°)		0 (Calculated)	0 (Calculated)	0 (Calculated)	0 (Calculated)
	Profile Evaluation	**Rolling Distance (mm)**	5,576	5,576	9,825	9,825
	Profile Start		5,033	5,033	9,335	9,335
	Face Width Position (mm)		0	0	0	0

Tip Right

Name			Sun		Plan
			Left Flank	Right Flank	Left
Linear	**Relief (µm)**		0	0	0
	Angle (°)		0 (Calculated)	0 (Calculated)	0 (Ca
	Profile Evaluation	**Rolling Distance (mm)**	5,576	5,576	9,82
	Profile Start		5,033	5,033	9,33
	Face Width Position (mm)		14	14	13
Parabolic	**Relief (µm)**		0	0	0
	Angle (°)		0 (Calculated)	0 (Calculated)	0 (Ca
	Profile Evaluation	**Rolling Distance (mm)**	5,576	5,576	9,82
	Profile Start		5,033	5,033	9,33
	Face Width Position (mm)		14	14	13

Root Left

Name			Sun		Planet	
			Left Flank	Right Flank	Left Flank	Right Flank
Linear	**Relief (µm)**		0	0	0	0
	Angle (°)		0 (Calculated)	0 (Calculated)	0 (Calculated)	0 (Calculated)
	Profile Evaluation	**Rolling Distance (mm)**	0,141	0,141	4,922	4,922
	Profile Start		0,685	0,685	5,413	5,413
	Face Width Position (mm)		0	0	0	0
Parabolic	**Relief (µm)**		0	0	0	0
	Angle (°)		0 (Calculated)	0 (Calculated)	0 (Calculated)	0 (Calculated)
	Profile Evaluation	**Rolling Distance (mm)**	0,141	0,141	4,922	4,922
	Profile Start		0,685	0,685	5,413	5,413
	Face Width Position (mm)		0	0	0	0

Root Right

Name			Sun		Plan
			Left Flank	Right Flank	Left
Linear	**Relief (µm)**		0	0	0
	Angle (°)		0 (Calculated)	0 (Calculated)	0 (Ca
	Profile Evaluation	**Rolling Distance (mm)**	0,141	0,141	4,92
	Profile Start		0,685	0,685	5,41
	Face Width Position (mm)		14	14	13
Parabolic	**Relief (µm)**		0	0	0
	Angle (°)		0 (Calculated)	0 (Calculated)	0 (Ca
	Profile Evaluation	**Rolling Distance (mm)**	0,141	0,141	4,92
	Profile Start		0,685	0,685	5,41
	Face Width Position (mm)		14	14	13

Bias

Name		Sun		Planet	
		Left Flank	Right Flank	Left Flank	Right Flank
Relief At Left Limit (ISO/AGMA/DIN) (µm)		0	0	0	0

Bias						
Relief At Right Limit (ISO/AGMA/DIN) (µm)			0	0	0	0
Pressure Angle Mod At Left Limit (mrad)			0	0	0	0
Pressure Angle Mod At Right Limit (mrad)			0	0	0	0
Lead Evaluation Left Limit (mm)			0	0	0	0
Lead Evaluation Right Limit (mm)			14	14	13	13
Profile Factor for 0 Bias Relief (%)			54,04	54,04	63,53	63,53
0 Bias Relief	**Rolling Distance (mm)**		3,078	3,078	8,037	8,037
Profile Evaluation Upper Limit			5,576	5,576	9,825	9,825
Profile Evaluation Lower Limit			0,141	0,141	4,922	4,922

Micro Geometry Overview

Mesh Micro Geometry	
Name	Micro Geometry 4
	Planet to Annulus

Micro Geometry			
Name		Planet	Annulus
Use Same Micro Geometry on Both Flanks?		No	No

Measured Micro Geometry					
Name		Planet		Annulus	
		Left Flank	Right Flank	Left Flank	Right Flank
Read Micro Geometry from an External File		Click To Open	Click To Open	Click To Open	Click To Open
Use Measured Map Data?		No	No	No	No

Central

Name		Planet		Annulus	
		Left Flank	Right Flank	Left Flank	Right Flank
Crowning Relief (µm)		5	5	0	0
Linear Relief (ISO/DIN/AGMA/VDI) (µm)		5	-5	0	0
Evaluation Left Limit (mm)		0	0	0	0
Evaluation Right Limit (mm)		14	14	15	15

Left Side

Name	Planet		Annulus	
	Left Flank	Right Flank	Left Flank	Right Flank
Linear Left Relief (µm)	0	0	0	0
Start Of Linear Left Relief (mm)	1,4	1,4	1,5	1,5
Evaluation Of Linear Left Relief (mm)	0	0	0	0
Parabolic Left Relief (µm)	0	0	0	0
Start Of Parabolic Left Relief (mm)	1,4	1,4	1,5	1,5
Evaluation Of Parabolic Left Relief (mm)	0	0	0	0

Right Side

Name	Planet		Annulus	
	Left Flank	Right Flank	Left Flank	Right Flank
Linear Right Relief (µm)	0	0	0	0
Start Of Linear Right Relief (mm)	12,6	12,6	13,5	13,5
Evaluation Of Linear Right Relief (mm)	14	14	15	15
Parabolic Right Relief (µm)	0	0	0	0
Start Of Parabolic Right Relief (mm)	12,6	12,6	13,5	13,5
Evaluation Of Parabolic Right Relief (mm)	14	14	15	15

Measured Micro Geometry

Name	Planet		Annulus	
	Left Flank	Right Flank	Left Flank	Right Flank
Use Measured Data?	No	No	No	No

Meshed Gear Information

Effective Face Width (mm)	b_{eff}	14

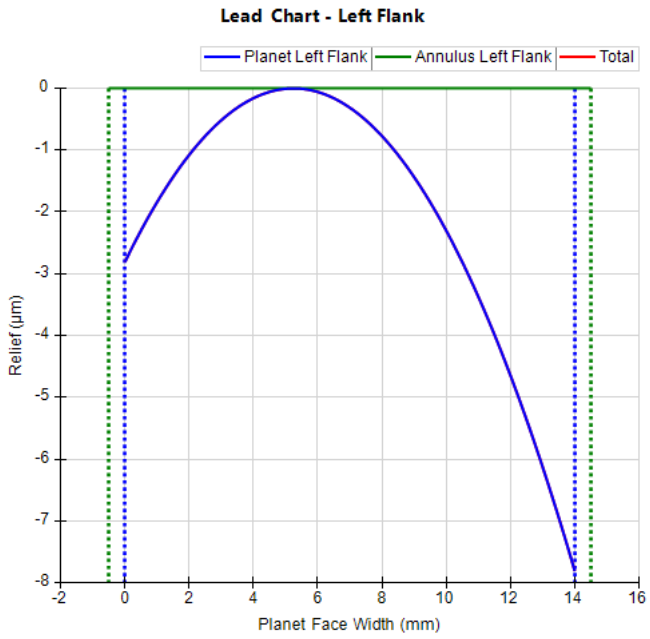

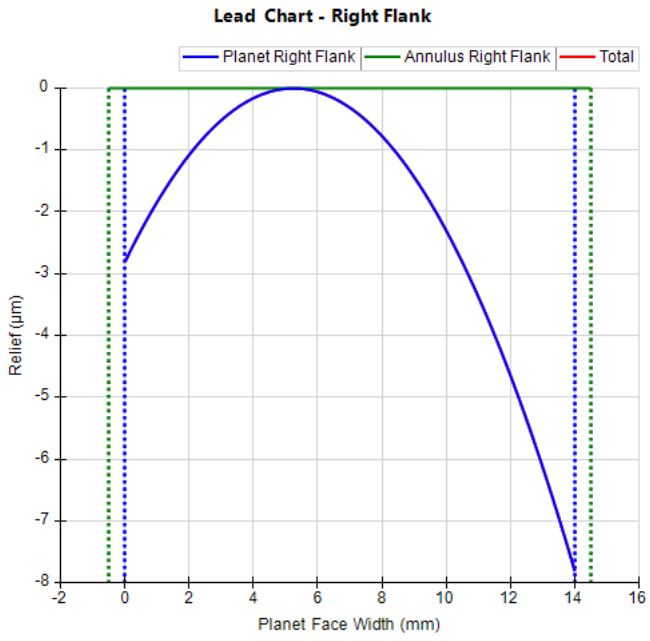

Main Profile

Name		Planet		Annulus	
		Left Flank	Right Flank	Left Flank	Right Flank
Barrelling Relief (µm)		14	14	0	0
Linear Relief (ISO/AGMA/DIN) (µm)		7	7	0	0
Location of Evaluation Upper Limit		User-Specified	User-Specified	User-Specified	User-Specified
Location of Evaluation Lower Limit		User-Specified	User-Specified	User-Specified	User-Specified
Evaluation Upper Limit	Rolling Distance (mm)	5,989	5,989	13,196	13,196
Evaluation Lower Limit		1,287	1,287	18,411	18,411
Main Profile Modification Ends at the Start of Tip Relief?		No	No	No	No
Main Profile Modification Ends at the Start of Root Relief?		No	No	No	No

Meshed Gear Information

Profile Measured As			Roll Distance	
Flank Name			Both Flanks	
Length of Contact (mm)			3,909	
Name			Planet	Annulus
Flank Name			Both Flanks	Both Flanks
Tip Form	Rolling Distance (mm)		5,989	13,196
End of Active Profile			5,989	13,196
Start of Active Profile			2,08	17,105
Root Form			1,287	18,411

Tip

Name		Planet		Annulus	
		Left Flank	Right Flank	Left Flank	Right Flank
Location of Tip Relief Start		User-Specified	User-Specified	User-Specified	User-Specified
Location of Tip Relief Evaluation		Tip Form	Tip Form	Tip Form	Tip Form
Linear Tip Relief (µm)		0	0	0	0
Linear Tip Relief Start	Rolling Distance (mm)	5,519	5,519	13,718	13,718
Linear Tip Relief Evaluation		5,989	5,989	13,196	13,196
Parabolic Tip Relief (µm)		0	0	0	0
Parabolic Tip Relief Evaluation	Rolling Distance (mm)	5,989	5,989	13,196	13,196
Parabolic Tip Relief Start		5,519	5,519	13,718	13,718

Root

Name		Planet		Annulus	
		Left Flank	Right Flank	Left Flank	Right Flank
Location of Root Modification Start		User-Specified	User-Specified	User-Specified	User-Specified
Location of Root Relief Evaluation		Root Form	Root Form	Root Form	Root Form
Linear Root Relief (µm)		0	0	0	0
Linear Root Relief Start	Rolling Distance (mm)	1,757	1,757	17,889	17,889
Linear Root Relief Evaluation		1,287	1,287	18,411	18,411
Parabolic Root Relief (µm)		0	0	0	0
Parabolic Root Relief Evaluation	Rolling Distance (mm)	1,287	1,287	18,411	18,411
Parabolic Root Relief Start		1,757	1,757	17,889	17,889

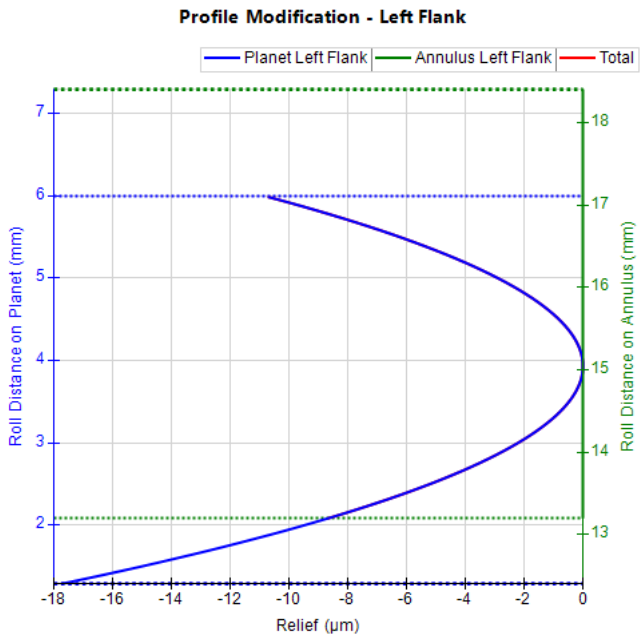

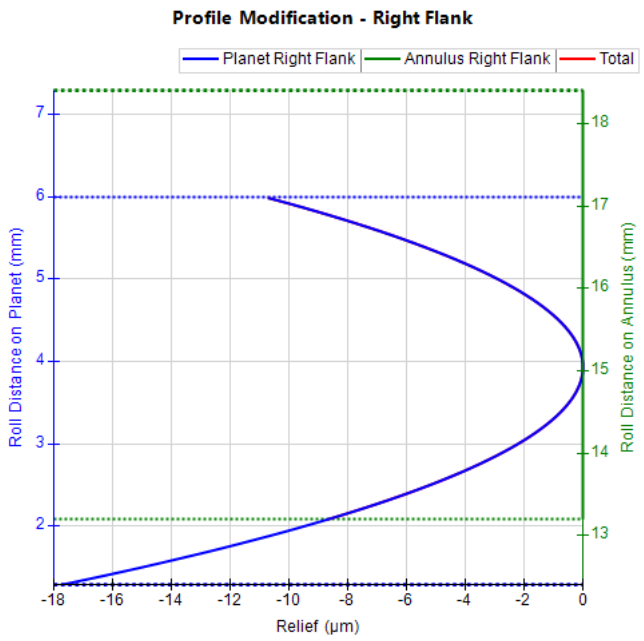

Measured Micro Geometry

Name	Planet		Annulus	
	Left Flank	Right Flank	Left Flank	Right Flank
Use Measured Data?	No	No	No	No

Tip Left

Name			Planet		Annulus	
			Left Flank	Right Flank	Left Flank	Right Flank
Linear	**Relief (µm)**		0	0	0	0
	Angle (°)		0 (Calculated)	0 (Calculated)	0 (Calculated)	0 (Calculated)
	Profile Evaluation	**Rolling Distance (mm)**	5,989	5,989	13,196	13,196
	Profile Start		5,519	5,519	13,718	13,718
	Face Width Position (mm)		0	0	0	0
Parabolic	**Relief (µm)**		0	0	0	0
	Angle (°)		0 (Calculated)	0 (Calculated)	0 (Calculated)	0 (Calculated)
	Profile Evaluation	**Rolling Distance (mm)**	5,989	5,989	13,196	13,196
	Profile Start		5,519	5,519	13,718	13,718
	Face Width Position (mm)		0	0	0	0

Tip Right

Name			Planet		Annu
			Left Flank	Right Flank	Left
Linear	**Relief (µm)**		0	0	0
	Angle (°)		0 (Calculated)	0 (Calculated)	0 (Ca
	Profile Evaluation	**Rolling Distance (mm)**	5,989	5,989	13,1
	Profile Start		5,519	5,519	13,7
	Face Width Position (mm)		14	14	15
Parabolic	**Relief (µm)**		0	0	0
	Angle (°)		0 (Calculated)	0 (Calculated)	0 (Ca
	Profile Evaluation	**Rolling Distance (mm)**	5,989	5,989	13,1
	Profile Start		5,519	5,519	13,7
	Face Width Position (mm)		14	14	15

Root Left

Name			Planet		Annulus	
			Left Flank	Right Flank	Left Flank	Right Flank
Linear	**Relief (µm)**		0	0	0	0
	Angle (°)		0 (Calculated)	0 (Calculated)	0 (Calculated)	0 (Calculated)
	Profile Evaluation	**Rolling Distance (mm)**	1,287	1,287	18,411	18,411
	Profile Start		1,757	1,757	17,889	17,889
	Face Width Position (mm)		0	0	0	0
Parabolic	**Relief (µm)**		0	0	0	0
	Angle (°)		0 (Calculated)	0 (Calculated)	0 (Calculated)	0 (Calculated)
	Profile Evaluation	**Rolling Distance (mm)**	1,287	1,287	18,411	18,411
	Profile Start		1,757	1,757	17,889	17,889
	Face Width Position (mm)		0	0	0	0

Root Right

Name			Planet		Annu
			Left Flank	Right Flank	Left
Linear	**Relief (µm)**		0	0	0
	Angle (°)		0 (Calculated)	0 (Calculated)	0 (Ca
	Profile Evaluation	**Rolling Distance (mm)**	1,287	1,287	18,4
	Profile Start		1,757	1,757	17,8
	Face Width Position (mm)		14	14	15
Parabolic	**Relief (µm)**		0	0	0
	Angle (°)		0 (Calculated)	0 (Calculated)	0 (Ca
	Profile Evaluation	**Rolling Distance (mm)**	1,287	1,287	18,4
	Profile Start		1,757	1,757	17,8
	Face Width Position (mm)		14	14	15

Bias

Name		Planet		Annulus	
		Left Flank	Right Flank	Left Flank	Right Flank
Relief At Left Limit (ISO/AGMA/DIN) (µm)		0	0	0	0

Bias						
Relief At Right Limit (ISO/AGMA/DIN) (µm)			0	0	0	0
Pressure Angle Mod At Left Limit (mrad)			0	0	0	0
Pressure Angle Mod At Right Limit (mrad)			0	0	0	0
Lead Evaluation Left Limit (mm)			0	0	0	0
Lead Evaluation Right Limit (mm)			14	14	15	15
Profile Factor for 0 Bias Relief (%)			35,17	35,17	82,06	82,06
0 Bias Relief	**Rolling Distance (mm)**		2,941	2,941	14,131	14,131
Profile Evaluation Upper Limit			5,989	5,989	13,196	13,196
Profile Evaluation Lower Limit			1,287	1,287	18,411	18,411

A.4 Comparison table

Comparison of component mass to Aune.

Table A.4: Mass comparison of components from Aune (Revolve NTNU) and this work (Lund Formula Student)

Revolve NTNU			
Component	**Amount**	**Weight (g)**	**Weight total (g)**
Sun gear	1	9,9	9,9
Large planet	3	122,7	368,2
Small planet	3	20,8	62,5
Ring gear	1	157,9	157,9
Planet pin shaft	3	38,9	116,8
Hub	1	307,4	307,4
Planet carrier	1	100,8	100,8
Pretention nut	1	36,2	36,2
Sum weight (g)			**1159,7**
Lund Formula Student			
Sun gear	1	11	11
Large planet + small planet	3	107	321
Ring gear	1	187	187
Planet pin	3	21	63
Hub	1	406	406
Planet carrier	1	90	90
Drive peg	3	7,5	22,5
Slotted pin	3	4	12
Sum weight (g)			**1112,5**

A.5 Bill of material

Table A.5: Bill of material

Component	Amount	Buy/Make	Supplier	Weight (g)	Weight total (g)
Carrier wheel	1	Make		406	406
Carrier motor	1	Make		90	90
Carrier bolt M5x40	3	Buy	Mattssons	8	24
Planet pin	3	Make		21	63
Drive peg	3	Make		7,5	22,5
Heli coil insert M5	3	Buy	Mattssons	1	3
Heli coil insert M8	3	Buy	Mattssons	2	6
Slotted pin ISO 8752, Obeh 8X18	3	Buy	Mattssons	4	12
Nord-lock washer M5	3	Buy	Nord-Lock	1	3
Sealing lid	1	Make		6	6
Bearings:					
NSK 6816VV	2	Buy	Nomo	150	300
SKF K 10X13X13 TN	3	Buy		2,3	6,9
SKF K 10X13X16 TN	3	Buy		2,9	8,7
Thrust washer	6	Make		1,7	10,2
Bearing spacer	1	Make		51	51
Sun gear	1	Make		11	11
Planets with shaft	3	Make		107	321
Ring gear	1	Make		187	187
Carrier seal Trelleborg TRA000800	1	Buy	Trelleborg	37	37
Sum weight gearbox					**1568,3**
Motor:					
Motor w/o housing	1	Buy	Fischer	2800	2800
Stator housing	1	Make		500	500
Rotor shaft	1	Make		157	157
Bearing shield gearbox	1	Make		90	90
Bearing shield connector	1	Make		90	90
Bearing NSK 6902VV	2	Buy	Nomo	15	30
Shaft seal Trelleborg TRAF00150	1	Buy	Trelleborg	5	5
Shield bolts M4x12	12	Buy	Mattssons	1,8	21,6
Brake button (modified top)	6	Make/buy	ISR	6	36
Brake button bolt M5x20 låg skalle	6	Buy	Mattssons	3,8	22,8
Metallic lock nut M5	6	Buy	Mattssons	1,5	9
MOTUL gear oil	1	Buy			
Safety wire for carrier bolts	1	Buy			
Epoxy for sealing lid	1	Buy			
Sum weight total, including motor components					**5329,7**